HHS Public Access

Author manuscript

Biomaterials. Author manuscript; available in PMC 2020 March 01.

Published in final edited form as:

Biomaterials. 2019 March ; 197: 146–160. doi:10.1016/j.biomaterials.2019.01.016.

Mesenchymal Stem Cell-Derived Extracellular Vesicles and Retinal Ischemia-Reperfusion

Biji Mathew, Ph.D.[1], **Sriram Ravindran, Ph. D**[*,3], **Xiaorong Liu, Ph.D.**[4], **Leianne Torres, M.D.**[1], **Mohansrinivas Chennakesavalu**[1], **Chun-Chieh Huang, PhD**[3], **Liang Feng, Ph.D.**[5], **Ruth Zelka, B.S.**[2], **Jasmine Lopez, B.S.**[1], **Monica Sharma, B.S.**[1], and **Steven Roth, M.D., F.A.R.V.O.**[*,1,2]

[1]Department of Anesthesiology, College of Medicine, University of Illinois at Chicago, Chicago, Illinois;

[2]Department of Ophthalmology and Visual Science, College of Medicine, University of Illinois at Chicago, Chicago, Illinois;

[3]Department of Oral Biology, College of Dentistry, University of Illinois at Chicago, Chicago, Illinois;

[4]Department of Biology, and Psychology, University of Virginia, Charlottesville, Virginia;

[5]Departments of Ophthalmology and Neuroscience, Northwestern University, Evanston, IL

Abstract

Retinal ischemia is a major cause of vision loss and impairment and a common underlying mechanism associated with diseases such as glaucoma, diabetic retinopathy, and central retinal artery occlusion. The regenerative capacity of the diseased human retina is limited. Our previous studies have shown the neuroprotective effects of intravitreal injection of mesenchymal stem cells (MSC) and MSC-conditioned medium in retinal ischemia in rats. Based upon the hypothesis that the neuroprotective effects of MSCs and conditioned medium are largely mediated by extracellular vesicles (EVs), MSC derived EVs were tested in an *in-vitro* oxygen-glucose deprivation (OGD) model of retinal ischemia. Treatment of R28 retinal cells with MSC-derived EVs significantly reduced cell death and attenuated loss of cell proliferation. Mechanistic studies on the mode of EV endocytosis by retinal cells were performed *in vitro*. EV endocytosis was dose- and temperature-dependent, saturable, and occurred via cell surface heparin sulfate proteoglycans mediated by the caveolar endocytic pathway. The administration of MSC-EVs into the vitreous humor 24 h after retinal ischemia in a rat model significantly enhanced functional recovery, and decreased neuroinflammation and apoptosis. EVs were taken up by retinal neurons, retinal ganglion cells,

[*]**Address correspondence to:** Steven Roth, M.D., F.A.R.V.O., Department of Anesthesiology, University of Illinois College of Medicine, 835 South Wolcott Avenue, Room E714, Chicago, Illinois 60612, rothgas@uic.edu, 312-996-0052 (telephone) 773-753-1024 (fax); Sriram Ravindran, Ph.D., Department of Oral Biology, University of Illinois College of Dentistry, 801 S Paulina St., Room 561C, Chicago, Illinois 60612, sravin1@uic.edu, 312-413-8167 (telephone).

Conflict of interest statement: None

and microglia. They were present in the vitreous humor for four weeks after intravitreal administration, with saturable binding to vitreous humor components. Overall, this study highlights the potential of MSC-EV as biomaterials for neuroprotective and regenerative therapy in retinal disorders.

Keywords

apoptosis; endocytosis; extracellular vesicles; electroretinography; exosomes; heparin sulfate proteoglycans; inflammation; ischemia; mesenchymal stem cells; microglia; neuroprotection; retinal ganglion cells; vitreous humor binding

Introduction

Age related macular degeneration, diabetic retinopathy, and glaucoma are the leading causes of irreversible blindness in Western countries, predicted to affect approximately 200 million people by 2020. Retinal ischemia and cell death resulting from, among other mechanisms, apoptosis and inflammation, are the hallmark events in the pathogenesis of the resulting visual loss [1, 2]. Current therapy focuses upon arresting disease progression using intraocular injections (e.g., anti-VEGF), eye drops, or surgery. Limitations of these treatments motivate studies of alternatives with greater safety margin, and higher likelihood of reaching the retinal target cells.

Successful strategies for enabling repair and regeneration of injured or diseased tissues should overcome the limitations of using morphogens and growth factors and rely on biomimetic strategies that minimize immunological and oncogenic consequences. In this regard, stem cell therapy using mesenchymal stem cells (MSCs) serves as an attractive option. MSCs are multipotent cells with regenerative and immunomodulatory properties[3, 4]. We have previously reported the robust neuroprotective effect of MSCs and their conditioned medium in an *in vivo* rat model of retinal ischemia-reperfusion injury [5–7]. In the eye, stem cell-based retinal cell replacement is a highly encouraging approach to trigger neuroprotection and/or regeneration [7]. However, low cell integration and aberrant growth, among other factors, limit its promise [8].

On the other hand, mounting evidence suggests that most MSC effects are paracrine in nature and are mediated by MSC derived extracellular vesicles (EVs) [9–11]. We and other groups have reported on the regenerative potential of MSC-EVs in soft and hard tissue regeneration [12–15]. Therefore, it may be possible to avoid the limitations and complications of stem cell therapy in the eye by using MSC derived EVs as biomimetic agents to aid neuroprotection and regeneration. This approach is made feasible by the fact that apart from possessing neuroprotective and regenerative properties, MSCs are also prolific producers of EVs [16]. Therefore, MSCs can prove to be an ideal source for therapeutic EVs that can be applied as naturally occurring biomaterials. Additionally, published studies show that EVs decrease neuronal cell death after hypoxia/ischemia *in vitro* and *in vivo*, stimulate axonal growth, and are anti-inflammatory and immunomodulatory, supporting a potential treatment role in retinal diseases [17–22]. Therefore, an aim of our

study was to test the hypothesis that MSC-EVs attenuate injury produced by hypoxia and ischemia in the retina.

EVs are integral to intercellular communication, interacting with recipient cells by three main mechanisms which resemble viral entry: 1) Binding surface receptors to trigger signal cascades, 2) internalization of surface-bound EVs via endocytosis, phagocytosis, or macro-pinocytosis, and 3) fusion with the cell to deliver material directly to the cytoplasmic membrane and cytosol [23]. Presently, there is a foundational knowledge gap with respect to the endocytosis of MSC-EVs by retinal cells and their mechanisms of entry. Uptake may depend upon proteins on the EV surface and the target cell [24]. A logical hypothesis is that cells use unique, and likely multiple, means to internalize EVs, e.g., integrins are necessary for EVs internalization in dendritic cells, macrophages [25], and heparin sulfate proteoglycans (HSPGs) for entrance into cancer cells [26, 27]. Moreover, clathrin- and caveolin-mediated pathways may be involved [28]. Therefore, one of the aims of this study was to evaluate the endocytic mechanism of MSC-EVs by retinal cells. These mechanistic studies help in developing a foundational knowledge of MSC-EV functionality in neuronal cells that can be exploited to promote enhanced delivery for engineered EVs as well as to facilitate cell-type specific targeting.

Compared to studies of neuronal injury *in vivo*, retinal neurons and other cells in the retina such as glial cells are more readily accessible by injection directly into the vitreous humor. Thus the retina is ideal as a window into the brain for studies of EV mechanisms and therapeutics [29] that targets neuroprotection and regeneration. This route is also commonly used in the treatment of retinal disease [30] and EV therapeutics should be optimized to use the intravitreal injections advantageously. However, the principles governing EV transit within tissues under normal and pathological conditions are poorly understood and are necessary to be determined in order to reach the full potential of EVs as effective biomaterials for ocular therapy.

Most pre-clinical studies use systemic administration of EVs. This is a low efficiency method as much of the injected dose is distributed outside of the target organ. For the retina, EVs delivered into the vitreous humor are expected to gain direct access to the inner retina cells including the retinal ganglion cells (RGCs). The vitreous humor is predominantly comprised of collagen and hyaluronic acid along with a network of extended random coil molecules that fills in the meshes of the collagen fiber network [31]. However, studies utilizing intravitreal injections of EVs have not focused on their interactions with the vitreous humor, their endocytic mechanisms and distribution within the eye [32, 33]. This knowledge is vital for understanding EV dynamics in the intraocular space and provides a foundational knowledge for nanoparticle-based biomaterials movement in this environment. Based on our earlier observation that MSC-EVs can bind to type I collagen [34], we hypothesized that the vitreous humor proteins can bind to EVs and serve as a reservoir for EVs prolonging their availability to retinal cells.

Overall, this study aims to evaluate the use of MSC-derived EVs as biomimetic agents for neuroprotection/regeneration following ischemic insult or injury using the eye as a model

system and characterizing the fundamental aspects of EV behavior within the eye and the retina in particular.

Materials and Methods

Isolation of human bone marrow mesenchymal cell derived EVs:

Human MSCs (hMSCs) were purchased from American Type Culture Collection (ATCC, Manassas, VA) and cultured in α-MEM supplemented with 20% FBS, 1% L-Glutamine, and 1% antibiotic-anti-mycotic solution (all from GIBCO, Thermo-Fisher). They were seeded to confluence and EVs were isolated from the culture medium as previously reported [13]. Briefly, cultures were washed with serum-free medium and cultured 48 h in the same medium under normoxic (21% O_2, 37°C) conditions. Conditioned medium was collected and centrifuged to remove whole cells and debris. After filtration with a 0.22-μm pore filter, supernatant was transferred to a 100-kDa molecular weight cut-off ultra-filtration conical tube (Amicon Ultra-15, Millipore, Burlington, MA), and centrifuged (3,000 × *g*) at 4°C for 45 min. EVs were isolated from the concentrated conditioned medium using Exo Quick-TC EV Precipitation Solution (System Biosciences, Palo Alto, CA) as we previously reported [34]. Isolated EVs were suspended in PBS, the suspensions normalized to cell number from the tissue culture plate from which they were isolated, and diluted such that 100 μl of suspension contained EVs isolated from 1 million cells. Cross-verification was performed by measuring RNA and total protein from EV suspensions to ensure that RNA/protein concentration from the same volume of EV remained consistent.

Characterization of MSC-EVs using electron microscopy, nanoparticle-tracking analysis, and Western blotting:

MSC-EVs isolated from the conditioned medium were characterized for size, morphology, and the specific exosome surface marker CD63 by transmission electron microscopy (TEM). CD63 and additional exosome surface markers were also examined using immunoblotting. Nanoparticle Tracking Analysis (NTA) by Nanosight (LM10-HS, Malvern, Westborough, MA) measured MSC-EV concentrations and particle size to confirm the composition and consistency of the MSC-EV preparations [35, 36].

MSC-EVs were adsorbed onto carbon-Formvar film grids and fixed in 2% glutaraldehyde/PBS at pH 7.4. Morphology was observed by TEM (80 kV, JEM-1220 TEM, JEOL, Peabody, MA), following staining with 2% phosphor-tungstic acid. For immunogold labeling, the MSC-EVs bound to the grids were permeabilized in 0.5% Triton X-100/PBS, then blocked with 5% BSA/PBS. The MSC-EVs were incubated for 2 h at room temperature in mouse monoclonal anti-CD63 (Abcam, Cambridge, MA, 1/100). Grids were washed three times and then incubated 1 h at room temperature in gold-labeled secondary antibody (1/2000, Abcam). The grids were then washed, dried and imaged using a JEOL JEM-3010.

For immunoblotting, the MSC-EV pellets were lysed in 1× RIPA buffer with protease and phosphatase inhibitor cocktail. Lysates were centrifuged at 4°C and protein concentrations measured using a protein assay kit (Pierce, Rockford, IL) Equal amounts of protein per lane (10 μg) were diluted with SDS sample buffer and loaded onto gels (4%–20% or 16%;

Invitrogen-Thermo Fisher). Proteins were electroblotted to polyvinylidene difluoride membranes (Immobilon-P; Millipore, Bedford, MA) with efficiency of transfer confirmed by Ponceau S Red (Sigma, St Louis, MO). Nonspecific binding was blocked with 5% nonfat dry milk in Tween-Tris-buffered saline. Membranes were incubated overnight at 4°C with primary antibodies: anti-CD81 (rabbit polyclonal, Abcam, 1/250), anti-CD63 (rabbit polyclonal, Abcam, 1/250), anti-CD9 (mouse monoclonal, Abcam, 1/250), and anti-α-HSP70 (rabbit polyclonal, System Biosciences, 1/1000 [37]. Anti-rabbit horseradish peroxidase (HRP)-conjugated (goat IgG; Jackson Immuno Research, West Grove, PA), or anti-mouse HRP-conjugated (sheep IgG; Amer-sham, Buckinghamshire, UK) secondary antibodies were applied at 1:20,000. Chemiluminescence was developed with a kit (Super Signal West Pico; Pierce). Protein bands were digitally imaged with a LICOR Odyssey (Lincoln, NE).

Fluorescent labeling of MSC-EVs:

To image MSC-EVs *in vivo* and *in vitro*, isolated EVs were labeled with green fluorescent-tagging reagent Exo-Glow Protein (System Biosciences), which labels intra-exosomal proteins fluorescently [13, 34, 38]. Briefly, MSC-EVs were suspended in PBS and incubated with Exo-Green Protein for 10 min at 37°C followed by 30 min incubation on ice. Labeled MSC-EVs were precipitated by adding Exo Quick-TC and centrifuged for 30 min at 14,000 × g. The obtained pellet was re-suspended in PBS.

Retinal cell line R28 culture:

Retinal cell line R28 was purchased from Kerafast (Boston, MA) and cultured according to the supplier's instructions. R28 is an adherent retinal precursor cell line derived from postnatal day 6 Sprague-Dawley rat retina immortalized with the 12S E1A gene, and has been used previously in studies on oxidative stress in retinal cells [39]. The 12S E1A gene was introduced via an incompetent retroviral vector; therefore, the cells produce no infectious virus. The cells have been passaged 200 times thus far, and show no signs of senescence. The heterogeneity of this cell line provides a diversity of cell types simulating *in vivo* retina and offers differentiation potential as an additional test of viability [40]. Cells were cultured in DMEM with 10% serum (420 ml DMEM incomplete, 15 ml 7.5% sodium bicarbonate, 50 ml calf serum, 5 ml MEM non-essential amino acids, 5 ml MEM vitamins, 5 ml L-glutamine (200 mM) and 0.625 ml Gentamicin (80 mg/ml), with pH adjusted to 7.4.

In vitro oxygen glucose deprivation model:

As an *in vitro* model of retinal ischemia, we used oxygen-glucose deprivation (OGD) in R28 cells. R28 cells were plated to reach 70% confluence in normal medium. For OGD, cells were cultured in glucose-free medium and subjected to hypoxia (1% O2, 5% CO2) for 24 h. Cells were then reoxygenated (21% O2, 5% CO2) for another 18 h, then assayed for lactate dehydrogenase (LDH, Promega, Madison, WI), and cell proliferation (ethynyl-deoxyuridine (EdU) assay followed by flow cytometry)[41, 42]. Cytotoxicity was assayed by using Sytox non-radioactive cytotoxicity assay kit (Promega). Briefly, culture supernatant samples from normoxic and OGD cells treated with MSC-EVs were transferred to a 96 well plate and equal volume of Sytox reagent was added, incubated 30 min at room temperature, and

absorbance measured at 490 nm. Percentage cytotoxicity was calculated from LDH release into the supernatant.

We used Click-iT EdU kit from Thermo-Fischer for measuring cell proliferation. Cells were labeled with EdU at the end of OGD and subjected to click reaction. The fluorescent signal generated by Click-iT EdU was detected by logarithmic amplification and analyzed by flow cytometry with a CyAn 2 Bench-top Analyzer (Beckman-Coulter, Brea, CA) [43].

Endocytosis experiments:

For imaging, R28 cells were seeded onto glass coverslips in 6-well tissue culture plates. At 24 h post-seeding, 50 μl of fluorescently labeled MSC-EVs (corresponding to EVs isolated from 500,000 hMSCs) or PBS was added to the culture medium and incubated for 1 h at 37°C. The PBS control was subjected to a similar labeling procedure as the EV suspension prior to being used in the experiment. After each experiment, coverslips were washed in PBS three times, fixed in 4% neutral buffered formalin, and immuno-labeled using anti-tubulin (1/5000, Sigma), anti-clathrin (1/500, Santa Cruz Biotechnology, Santa Cruz, CA), or anti-caveolin-1 (1/1000, Santa Cruz) as previously described [13]. Slides were imaged using a Zeiss (Thornwood, NY) LSM 710 confocal microscope or Zoe fluorescent imager (BioRad, Hercules, CA).

Quantitation of endocytosis and dose-dependency experiments were performed in 96 well ELISA plates, with 10,000 R28 cells per well. At 24 h post seeding, increasing amounts of MSC-EVs were added and incubated for 1 h at 37°C. For blocking experiments, 20 μl of MSC-EVs were used per 20,000 cells (2× saturation). Cells were pre-treated with either heparin (0, 5 and 10 μM, Sigma), RGD (Arg-Gly-Asp peptide, 0, 0.5, 1, and 2 mM, Abcam), MBCD (Methyl-β-cyclodextrin, 0, 2.5, 5 mM, Sigma), or incubated at 4°C for 1 h followed by incubation with the MSC-EVs. The experiments were conducted in quadruplicate. Wells were washed 3 times in PBS, fixed using 4% neutral buffered forma lin, and the fluorescence measured using a BioTek (Winooski, VT) 96 well plate reader equipped with the appropriate band pass filter sets.

In vivo rat model of retinal ischemia:

Procedures conformed to the Association for Research in Vision and Ophthalmology Resolution on the Use of Animals in Research (https://www.arvo.org/About/policies/statement-for-the-use-of-animals-in-ophthalmic-and-vision-research/) and were approved by our Animal Care Committee. Male Wistar rats (200–250 gm, Harlan, Indianapolis, IN) were maintained on a 12 h on/12 h off light cycle. For retinal ischemia, rats were anesthetized with ketamine 100 mg/kg, and xylazine, 7 mg/kg intraperitoneally (i.p.). After sterile preparation, and working under an operating microscope, a 30-gauge, 5/8-inch metal needle (BD Precision Glide, Becton-Dickinson, Franklin Lakes, NJ) was placed with its tip inside the anterior chamber of the eye. The needle was connected by plastic tubing via a three-way stopcock to a pressure transducer (Trans-pac, Hewlett-Packard) and an elevated bag of balanced salt solution (BSS; by sterile technique BSS was transferred from its bottle (Alcon, Ft Worth, TX) to an empty 1000 ml 0.9% saline plastic bag. Intraocular pressure (IOP), continually displayed on an anesthesia monitor (Hewlett-Packard HP78534C), was increased

to 130–135 mm Hg for 55 min by pressurizing the bag (Smiths Medical Clear Cuff, Minneapolis, MN). The eyes were treated with topical Vigamox (0.5%; Alcon), cyclomydril (Alcon) and proparacaine (0.5%; Bausch & Lomb, Bridgewater, NJ). Temperature was maintained at 36–37°C using a servo–controlled heating blanket (Harvard Apparatus, Holliston, MA). Oxygen saturation of the blood was measured with a pulse oximeter (Ohmeda-GE Healthcare, Madison, WI) on the tail. Supplemental oxygen, when necessary to maintain O_2 saturation > 93%, was administered with a plastic cannula placed in front of the nares and mouth.

Electroretinography:

Our procedures have been described in detail previously [44–46]. Briefly, for baseline and post–ischemic follow–up electroretinography (ERG), rats were dark adapted and were injected i.p. with ketamine (35 mg/kg) and xylazine (5 mg/kg) every 20 min to maintain anesthesia. Custom Ag/AgCl electrodes were fashioned from 0.01 inch Teflon-coated silver wire (Grass Technologies, West Warwick, RI). Approximately 10 mm was exposed and fashioned into a small loop to form the corneal/positive electrodes while ~20 mm was exposed to form a hairpin loop, the sclera/negative electrodes looped around the eye. To maintain moistness of the cornea and electrical contact, eyes were treated intermittently with Goniosol (Alcon). Electrodes were referenced to a 12 mm × 30-gauge stainless steel, needle electrode (Grass) inserted 2/3 down the length of the tail. Stimulus-intensity ERG recordings were obtained simultaneously from both eyes using a UTAS-E 4000 ERG system with a full-field Model 2503D Ganzfeld (LKC Technologies, Gaithersburg, MD) as previously described [6, 47, 48].

The ERG a- and b-waves were expressed as normalized intensity-response plots with stimulus intensity (log cd s/m^2) on the X-axis, and corresponding percent recovery of baseline on the Y-axis, as we previously reported [6, 49, 50]. Recorded amplitude, time course, and intensity were exported and analyzed in Matlab 2011a (MathWorks, Natick, MA) as previously described [6, 48–50]. ERG waveform recovery after ischemia was corrected for day-to-day variation and reference to the non-ischemic eyes as previously described [5, 7].

In vivo administration of MSC-EVs, and MSC-EV depleted conditioned medium into the eyes:

MSC-EV-depleted conditioned medium was prepared by isolating MSC-EVs from the medium as described above and served as control in addition to PBS. The conditioned medium was centrifuged, filtered to remove cells and debris, and concentrated using 10-kDa molecular weight cut-off ultra-filtration conical tubes (Amicon Ultra-15) by centrifuging at 3,000 × *g* at 4°C for 45 min. MSC-EVs were isolated as described above. Supernatant without MSC-EVs was evaluated for pH, and for protein concentration using a protein assay kit (Pierce). Normoxic MSC-EV-depleted conditioned medium (10 μg protein/4 μl), MSC-EVs (4 μl of 1×10^9 particles/ml), or PBS (4 μl) were injected into the vitreous humor of both the ischemic (right) and non-ischemic (left) eyes, 24 h after retinal ischemia as we previously described (previously we had determined that 4 μl was the maximal safe volume for injection into the vitreous humor in rats [6]). The normal/non-ischemic left eye served as

the control eye. Rats were subjected to ERG recordings at baseline, prior to ischemia, and at seven days post injections, i.e., 8 days after ischemia.

Evaluation of apoptosis and inflammatory markers in MSC-EV injected retinae:

Retinal tissue was homogenized with a Bead-Bug Micro-tube Homogenizer (Midwest Scientific, Valley Park, MO) in RIPA buffer (Cell Signaling Technology, Danvers, MA) containing protease and phosphatase inhibitors. Lysates were centrifuged at 4°C and protein concentration measured using a BCA protein assay kit (Pierce). Equal amounts of protein (15 μg) were loaded onto 10% sodium dodecyl sulfate–polyacrylamide gel electrophoresis gels, transferred onto nitrocellulose membranes and Western blotting was performed as we previously reported [7]. Membranes were probed with anti-IL-6 (Santa Cruz, mouse monoclonal, 1/500, anti-TNF-α (Santa Cruz, mouse monoclonal, 1/500), and anti-cleaved caspase-3 (Cell Signaling, rabbit polyclonal, 1/1000) primary antibodies. IL-6 and TNF-α are markers of inflammation, and caspase-3 of apoptosis gene-related expression [51]. Band density was calculated using densitometry with macros in ImageJ (https://imagej.nih.gov/ij/docs/guide/user-guide-USbooklet.pdf) where each protein was normalized to anti-β-actin, as previously reported [7].

Fundus imaging and in vivo tracking of MSC-EVs in the eye:

To track MSC-EVs *in vivo*, the EVs were labeled with Exo-Glow Protein prior to intravitreal injection. The labeled MSC-EV pellet was suspended in PBS and injected (4 μl of 1×10^6 particles/ml) 24 h post-ischemia into the mid-vitreous under direct vision using an operating microscope, in both normal and ischemic eyes [7]. For *in vivo* real-time imaging, rats were injected i.p. with ketamine (35 mg/kg), and xylazine (5 mg/kg). Pupils were dilated with 0.5% tropicamide (Alcon), and cyclomydril. Fluorescent fundus images were obtained using a Micron IV Retinal Imaging Microscope (Phoenix Research Labs, Pleasanton, CA), at 1, 3, 7, 14, and 28 days after injections into the vitreous humor as we previously reported [7].

Fluorescent imaging and localization of labeled MSC-EVs in retinal flat mounts:

Exo-green MSC-EV-injected ischemic and normal rats were anesthetized at different time points (1, 3, and 7 days) after intravitreal injections and subjected to whole animal perfusion-fixation with PBS and 4% paraformaldehyde [52]. Following enucleation, the eye cups were prepared by removing the cornea, lens and vitreous. The eyecups were post-fixed in 4% PFA for 30 min, washed twice in PBS, and permeabilized with PBST (0.3% Triton X-100 in PBS, twice). The eye cups were blocked overnight in 2% Triton X-100, 10% normal serum and 1 mg/ml BSA [53]. The primary antibodies anti-IBA-1 for retinal microglia [54] (1:500, Novus Bio, Littleton, CO), and anti-Brn-3a for retinal ganglion cells [55](1:500, EMD Millipore), and anti-β-tubulin III for retinal neurons [56] (1:500, Sigma), were incubated with the eyecups at 4°C for 48 h followed by washing and incubation with the appropriate secondary antibodies (Alexa Fluor 555 and 647, Molecular Probes, Thermo-Fisher) for an additional 48 h at 4°C. The samples were washed again, and the retinal tissues carefully dissected from the choroid and placed on a glass slide and mounted with Pro-Long Diamond Antifade Mounting Solution with DAPI (Life Technologies, Thermo-Fisher). Slides were imaged using a Zeiss 710 confocal at 63 and 100× oil immersion magnification, and images deconvoluted using Zeiss Zen v2.4 software.

Fluorescent TUNEL:

Fluorescent TUNEL (terminal deoxynucleotidyl transferase-mediated dUTP nick end labeling assay) was performed with Apop Tag Red In Situ Apoptosis Detection Kit (Millipore-Sigma) on 7 μm thick cryosections at 24 h post-MSC-EV injection (48 h after ischemia). This is consistent with the time course of apoptosis that we previously described in retinal ischemia, where peak TUNEL was present 48 h after ischemia [57, 58]. Briefly, cryosections were fixed and hydrated in 4% paraformaldehyde followed by ethanol: acetic acid (2:1) post fixation. Sections were then exposed to equilibration buffer and incubated in TdT enzyme for 1h in a humidified chamber followed by application of anti-digoxigenin conjugate for 30 min at room temperature, with the slides covered to protect them from light exposure. Sections were mounted using Prolong Diamond Antifade Mounting Agent containing DAPI.

Imaging was performed at 20× magnification on a Zeiss Axiovert 100 inverted microscope using Metamorph 7.3. The images were processed and analyzed using ImageJ similar to our previous descriptions [6]. In brief, the inner and outer nuclear retinal cell counts for DAPI (total cell nuclei), and the TUNEL stained nuclei were counted using an automated cell counting macro in ImageJ, utilizing the Cy3 channel. The TUNEL cells of the retinal ganglion cell (RGC), inner nuclear, and outer nuclear layers were counted blindly without knowledge of the group name.

MSC-EV vitreous humor binding assay:

The vitreous humor was extracted from normal rat eyes. After measuring the protein concentration, dilution to 50μg/100 μl was performed in coating buffer (0.2M sodium bicarbonate, pH 9.4) and 96 well plates were coated with the vitreous proteins overnight at 4°C. Plates were washed and incubated for 1 h at room temperature with increasing amounts of fluorescently labeled MSC-EVs as described previously [34]. Fluorescence from the bound MSC-EVs after washing was measured using a BioTek ELISA plate reader with the appropriate band pass filter sets and the results were plotted against MSCEV amount to obtain the binding curves.

Statistical Analysis:

Briefly, data were expressed as mean ± standard deviation (SD), and compared by ANOVA where appropriate, and by t-testing as reported previously [7]. Analyses were performed using Stata version 10.0 (College Station, TX).

Results

Characterization of MSC-EVs:

The purified MSC-EVs were characterized by NTA, immunoblotting, and EM. EVs are a complex mixture of membrane-bound vesicles released from most cells, and according to their size they have been classified as microvesicles (100–800 nm), exosomes (50–150 nm), and the much larger apoptotic bodies [59]. MSC-EVs were found to be exosomal in their size and properties. Analysis of size and concentration of isolated EVs using NTA demonstrated a bell-shaped curve with the majority of the area under the curve falling within

the characteristic exosomal size range of 50–150 nm, a peak at 89 nm, and a modal size of 93 nm. Another peak at 141 nm likely represents a mixture of exosomes and microvesicles, and the smaller peak at 324, the less abundant microvesicles (Fig 1A). Western blot demonstrated exosome surface markers CD81, CD63, CD9, and HSP70α in the exosomal lysates, and not in exosome-depleted conditioned medium (Fig 1B). The exosomal lysates were probed for tubulin as negative control for intracellular protein and no positive staining was observed (data not shown). TEM (Fig 1C) showed particle shape and diameter of approximately 100 nm consistent with exosomes, and immuno-gold EM labeling for CD63 (Fig 1D) showed the presence of CD63 on the exosome surface, confirming the immunoblotting results and that exosomes constitute most of our MSC-EVs in agreement with other studies [60].

MSC-EVs are endocytosed by R28 retinal cells via specific mechanisms:

These experiments were performed to identify the basic mechanisms that control MSC-EV internalization by retinal cells. We first confirmed that MSC-EVs are endocytosed by R28 retinal cells. Fig 2A is a representative confocal image demonstrating that fluorescently labeled MSC-EVs were endocytosed by R28 cells in culture. Most of the R28 cells contained MSC-EVs indicating a high uptake efficiency. The MSC-EVs were visualized as punctate staining as well as agglomerates within the cells and across the nuclei. Yellow or orange staining in the composite image (lower right panel of Fig 2A) indicated overlap with tubulin, showing that MSC-EVs were in the cytoplasm. Fig 2B shows dose-dependent, saturable endocytosis of fluorescently labeled MSC-EVs. Furthermore, endocytosis was reduced significantly at 4°C, indicating temperature dependence (Fig 2C). Taken together, these results indicate the presence of a controlled, energy-dependent endocytic mechanism for MSC-EVs in retinal cells.

Next we aimed to identify the endocytic receptors. Studies have shown involvement of integrins in EV endocytosis in some cell types [24, 25]. To analyze integrin involvement in the endocytosis of MSC-EVs by R28 retinal cells, integrins on the R28 cell membrane were blocked by pre-treatment with increasing concentrations of the integrin-binding Arginyl-glycyl-aspartic acid (RGD) peptide. No statistically significant impact upon MSC-EV endocytosis was observed (Fig 3A). Conversely, when MSCEVs were pre-treated with heparin to mimic the binding to HSPGs on the R28 plasma membrane,[26] EV endocytosis was significantly and dose-dependently blocked (Fig 3B). Confocal microscopy qualitatively confirmed these quantitative results (Figs 3C–E). The results ruled out integrin involvement in the endocytosis of MSC-EVs and indicated a role for cell surface HSPGs.

Depending on the receptors involved and the type of ligand, endocytosis can occur via a clathrin or caveolin-mediated process [61]. Endocytosed MSC-EVs were analyzed by confocal microscopy for co-localization with caveolin-1 (a marker for caveolae and lipid rafts) and clathrin (which forms clathrin-coated endocytic pits) [61]. Representative confocal images (Figs 4A–B) show co-localization of the endocytosed MSC-EVs (green) with caveolin-1 (red). No co-localization was observed with clathrin (red) in Figs 4C–D. Blocking caveolar-mediated endocytosis by MBCD, to disrupt membrane cholesterol [62], dose-dependently inhibited MSC-EV endocytosis (Figs 4E–F, and Fig 4G).

MSC-EVs attenuate cell death in R28 cells subjected to OGD *in vitro*:

Oxygen glucose deprivation (OGD) results in cell death and mimics ischemic conditions *in vitro* [63]. We tested the hypothesis that MSC-EVs rescue R28 cells from OGD-mediated cell death. R28 cells pre-treated for 24 h with or without varying doses of MSC-EVs were subjected to OGD. Fig 5A shows that in the absence of MSC-EVs, OGD induced cytotoxicity was > 75%. Cytotoxicity was significantly reduced in a dose-dependent and saturable fashion with MSC-EV pre-treatment. To evaluate the effect of MSC-EVs on the proliferative state of R28 cells, flow cytometry analysis was performed for EdU positive cells (Figs 5B&C) under both normoxic and OGD conditions. Under normoxic conditions, the percentage of EdU positive cells was no different between PBS control, MSC conditioned medium, EVs, or EV depleted conditioned medium. A slight decrease in the percentage of proliferating cells was observed with the EVs although this change was not significant. Conditioned medium as well as EVs significantly improved the number of proliferating cells under OGD conditions. When conditioned medium depleted of EVs was used, the protective effect was abrogated suggesting that the protective effect is likely due to EVs in the conditioned medium.

MSC-EV administration following retinal ischemia *in vivo* attenuates ischemic damage:

We tested the hypothesis that MSC-EVs reverse the effects of ischemic injury *in vivo* in a rodent model. MSC-EVs injected intra-vitreally 24 h after ischemia significantly improved the recovery of the a- and b-wave amplitudes of the ERG in comparison to both PBS vehicle and EV-depleted conditioned medium from MSCs (Figs 6A–B). Electroretinogram (ERG) results were normalized to control eyes and to the baseline prior to ischemia as previously described [6, 47, 48], which accounts for day-to-day variation in the amplitudes of the non-ischemic eyes. Y axis is % recovery relative to baseline/100 and x-axis is stimulus intensity in log cd-ms/m^2. The amplitudes are shown as mean ± SD. There was significant improvement of recovery of the a-wave amplitude with intravitreal MSC-EVs vs PBS control, and significant improvement of recovery of the b-wave amplitude with intravitreal MSC-EVs compared to PBS and MSC-EV-depleted medium controls.

The significant improvement of the a- and b-waves is also evident in the representative ERG stimulus-intensity traces shown in Fig 6C. To evaluate if the MSC-EV functionality was related to its anti-apoptotic effects, we quantitated fluorescent TUNEL on retinal cryosections (Figs 7A–B). MSC-EV injection 24 h after ischemia significantly reduced TUNEL in the inner and outer nuclear layers and in the retinal ganglion cell layers. There was an increase in TUNEL in the RGC, but not in other cell layers in MSC-EV-injected non-ischemic retinae. In whole retinal homogenates, levels of the inflammatory mediumtors TNF-α and IL-6 were significantly reduced upon MSC-EV treatment following ischemic injury *vs* vehicle controls (Figs 8A–C). There was also a significant reduction in cleaved caspase-3 levels in MSC-EV treated ischemic retina *vs* vehicle controls (Figs 8A and D). In non-ischemic MSC-EV injected retinae, there was no significant change in levels of any of the three proteins, although cleaved caspase 3 was observed with EV or PBS treatment under non-ischemic conditions, there was no statistically significant increase with respect to PBS control. Taken together, the results in Figs 6–8 indicate that MSC-EV treatment following retinal ischemia leads to functional improvement in the retina via reduction of apoptosis and

neuroinflammation. In addition, the results indicate, that with the exception of an increase in TUNEL in the RGC layer, no evidence of inflammation or apoptosis triggered by EVs in normal retina was detected by our measurement techniques.

MSC-EV uptake and distribution in retina *in vivo*:

Having observed the functionally neuroprotective effects of MSC-EVs in the ischemic retina, we evaluated the distribution of the EVs after injection into the vitreous humor. Fig 9A displays localization of labeled MSC-EVs in the vitreous humor and retina. There was persistent retention of MSC-EVs in vitreous humor up to 4 weeks after intra-vitreal injection. Ischemic retina demonstrated increased MSCEV uptake *vs* control non-ischemic eyes. In addition, we also observed large deposits of accumulated MSC-EVs in the control and ischemic retina. These results are entirely explainable as fluorescence from the MSC-EVs, as previously it has been shown that fluorescein injected into the vitreous humor is cleared within 48 h [64]. To test the vitreous humor's capacity as a reservoir for MSC-EVs, quantitative binding experiments were performed on assay plates coated with protein isolate from the vitreous humor and increasing dose of fluorescently labeled MSC-EVs. Results presented in Fig 9B illustrate dose-dependent and saturable binding of MSC-EVs to vitreous humor proteins. This result explained the presence of accumulated MSC-EVs in the vitreous humor.

To evaluate if MSC-EVs are preferentially endocytosed by specific retinal cells *in vivo*, retinal flat mounts prepared at different time intervals after fluorescently labeled MSC-EV injections were immuno-stained with markers for different retinal cells. Brn3A was used as the marker for RGCs and IBA-1 for retinal microglial cells. Flat mounts (Fig 10A) showed distribution throughout the retina and persistence of MSC-EVs at one week after injection (time points later were not evaluated). Fig 10B shows that both RGCs and microglia take up MSC-EVs. Moreover, Figs 10A and B qualitatively show greater microglial amoeboid, or activated morphology in ischemic, non-MSC-EV treated retinae *vs* MSC-EV-treated retinae, suggesting reduced microglial activation in ischemia in the presence of MSC-EVs.

Fig 11 contains 100× confocal microscopic images of retinal flat mounts from non-ischemic (upper panels) and ischemic retinae (lower panels) respectively from retinal tissues harvested 24 h after administration of MSC-EVs, that corresponds to 48 h after ischemia. MSC-EVs are present in retinal neurons, as indicated by presence of MSC-EVs in cells labeled with specific neuronal marker β-tubulin III (Fig 11E) as well as in axonal or dendritic projections (arrows in Fig 11E) and in Brn3a-positve cells (Fig 11F) indicating that the MSC-EVs are endocytosed by the retinal neurons and by RGCs.

Discussion

In this study, we present new data on the neuroprotective effects of MSC derived EVs in the retina that are relevant to treatment of ischemia-related retinal degeneration, as well as to the treatment of neuronal injuries in general. We referred to our vesicular populations as MSC-EVs. Although the definition of exosomes is evolving, a modal size of 93 nm along with the expression of exosome specific markers indicate that our population is predominantly exosomes as defined by Kowal et al [65]. These studies using MSC-EVs depict a consistent

progression from stem cell-based therapy to cell-free therapy for retinal tissue neuroprotection and regeneration [66] and regenerative medicine in general. As cell-free therapy, MSC-EVs offer a safe, biomimetic alternative with lower oncogenic and immunological risks and greater target specificity [67]. To date, only a small number of studies have examined EV therapy in the retina, one demonstrating therapeutic effect in an optic crush model and the other in a glaucoma model [32, 33], both in rats. However, to our knowledge, no prior studies have examined the mechanisms of uptake of EVs in retina, their vitreous humor and cellular distribution, nor effects upon ischemic insult.

Our results indicate that EVs are endocytosed by retinal R28 cells in a dose-dependent, saturable, and temperature-dependent manner, suggesting the involvement of a receptor-mediated endocytic mechanism. Published studies show that EVs from different sources undergo endocytosis via different mechanisms owing to a change in the composition of the EV membrane. The clathrin and caveolar pathways, phagocytosis, and macro-pinocytosis have all been implicated in endocytosis of EVs [24, 68, 69]. Our results indicated that MSC-EVs are endocytosed by R28 retinal cells via the caveolar endocytic pathway mediated by cell surface HSPG receptors. Quantitative studies showed that MSC-EV endocytosis by R28 cells was dose-dependently blocked by disrupting the cell membrane cholesterol or by competitively blocking HSPG binding sites on the EVs with heparin. Furthermore, confocal microscopy revealed that membrane bound and endocytosed EVs co-localize with caveolin-1, further confirming the role of the caveolar endocytic process. Considering that the caveolar pathway routes its cargo away from lysosomal degradation and considering the functional activity of the endocytosed EVs, it is possible that for the EVs to be functionally active, this mode of endocytosis is ideal.

These mechanistic studies highlight the potential of MSC-EVs as biomimetic agents for treatment of neurodegenerative diseases and nerve injuries in general. From a therapeutic perspective, the effectiveness of MSC-EVs is dependent on the efficiency of endocytosis by target cells. Improved endocytic efficiency can promote greater target-specificity at the site and reduce ectopic effects. Therefore, our results outlining the endocytic mechanism open up avenues for future studies that can be aimed at engineering EVs for enhanced delivery by targeting these endocytic pathways. In addition, they can also serve as quality control points for function-specific engineered exosomes to ensure that intrinsic endocytic processes are not altered upon generation of engineered EVs. However, the R28 cell line is an immortalized retinal cell line that displays both neuronal and glial cell properties [40, 70]. While the ability of these cells to proliferate enables measurement of a critical cell function, further studies using primary retinal cells may be required to confirm the endocytic mechanism identified here.

In the *in vitro* OGD model, results indicated a dose response effect of MSC-EVs and saturation that corroborates well with our endocytosis data. Furthermore, cytotoxicity studies using quantitation of proliferative cells via flow cytometry revealed that MSC-EVs rescue the R28 cells from OGD insult. Taken together, these studies showed that MSC-EVs have the potential to promote the survival and proliferation of retinal neurons that have been subjected to ischemia-type stress *in vitro*. These results encouraged the evaluation of MSC-EVs post ischemic insult *in vivo* in a rodent model.

The onset of retinal ischemic injury *in vivo* is manifested as neuronal cell death, apoptosis, and neuroinflammation resulting in RGC loss, blood-retinal barrier permeability, and neurodegeneration [7]. Therapeutic effects of MSC derived EVs are reported in a wide range of inflammatory diseases including, but not limited to ischemia-reperfusion injury in brain, heart, kidney [71–73] as well as in neurodegenerative diseases [66, 74]. Our results demonstrate that MSC-EVs render their neuro-protective effect by decreasing neuroinflammation and neuronal apoptosis. These results provide an insight into the mechanism behind MSC-EV action in the retina under ischemic injury and serve as a foundational knowledge that can be used to generate engineered EVs with function-specific miRNA cargo with antiinflammatory and anti-apoptotic properties.

Prior to the current study, the uptake, retention, turnover and prolonged effect of EVs in the retina have been addressed in only a limited manner. The role of the vitreous humor in EV retention and the subsequent endocytosis by different cells of the retina has remained unexplored. A few recent studies injected EVs in single dose, weekly, and monthly in a model of glaucoma, and reported enhanced protection with multiple administration, [32] while another group reported high dose, single injection EV (15×10^9 particles/ml) induced protection in experimental autoimmune uveitis [75]. To our knowledge dose dependence and toxicity studies using MSC EVs with retinal or neuronal cells under normal and ischemic conditions has not performed. Our results using concentrated EV injections in an *in vivo* model did not cause any deleterious effect in the ERG functional studies, nor increased inflammatory mediators. Additionally, our *in vitro* and *in vivo* results indicate a mild level of toxicity of MSC EVs under normoxic conditions albeit being statistically insignificant. However, there was no corresponding increase in the inflammatory markers or increase in cleaved caspase 3 in retinal homogenates in the normal non-ischemic retinae. Further studies will be required to evaluate if there is any functional effect of EVs specifically on the retinal ganglion and amacrine cells in the RGC layer.

Multiple dosing or higher doses are not required if EVs can traverse the vitreous and reach target cells in the inner retina after administration. Greater quantities of MSC-EVs were observed in ischemic compared to non-ischemic retinae. Additionally, they were more concentrated in RGCs and in microglial cells. This increase in the uptake of EVs by ischemic cells is potentially advantageous, but the mechanism of this effect requires further investigation. Preferential uptake by cells in ischemic neuronal and glial has potentially important implications in therapeutic development of EVs as biomimetic agents for treatment of nerve injuries and neuro degenerative diseases. Likewise, a surprising result was that while EVs robustly attenuated TUNEL throughout the retina and decreased cleaved caspase 3 presence indicating a decrease in apoptosis, the labeled EVs were not found deeper than the retinal ganglion cell layer at the time of peak apoptosis (48 h after ischemia). This suggests that the EV effects on apoptosis are either due to altered retinal cell-to-cell signaling, e.g., via Muller glial cells that traverse most of the retina,[76] or are due to release of EV induced anti-apoptotic factors from the cells that have endocytosed them. It is also possible that with more time, the MSC-EVs penetrate more deeply into the retina, and further studies will be required to test this hypothesis.

We showed specific uptake of MSC-EVs *in vivo* by RGCs and microglia, as well as by retinal neurons. The targeting of RGCs by the EVs supports development of EVs and engineered EVs for the treatment of glaucoma and other diseases of optic nerve that result in degeneration of RGCs. These studies may also serve as a prelude to neuro-targeted EV therapy for treatment of specific nerve cells. It is interesting that MSC-EVs were present in axonal or dendritic projections from RGCs and retinal neurons. Further studies are necessary to determine if the MSC-EVs are transported along the axons, as this may enable novel access to the optic nerve via retrograde transport [52]. Microglial activation was not quantitated in this study but decreased amoeboid formation after ischemia in MSC-EV-injected eyes suggests another potential target for MSC-EV-therapy. Microglial activation in the retina may be a pathogenic factor in various diseases including diabetic retinopathy, glaucoma, and age-related macular degeneration, thus MSC-EVs targeting microglia could be a novel treatment modality [77, 78].

Our study indicates that intravitreal injection produced uptake of MSC-EVs uniformly in the retina (as seen in the distribution on flat mounting). The MSC-EVs remained in the vitreous humor for up to 4 weeks after injection and quantitative binding experiments to vitreous humor-derived proteins suggest that the effect is due to binding to vitreous humor proteins in a dose-dependent and saturable manner. As a result, the vitreous humor serves as a reservoir for release of EVs into the retina and this property could be used advantageously to prolong EVs effects and minimize the number of injections necessary to produce long-term effects.

One of the significant challenges associated with the use of EVs for therapeutic purposes is the ability to deliver them site specifically to relevant tissues. From this perspective, the identification of EV binding kinetics to vitreous proteins is valuable data for the biomaterials community. We predict that future studies aimed at identifying peptide sequences present in vitreous collagens can be used to generate engineered biomimetic matrices used to deliver EVs and possibly promote controlled release of EVs to aid repair and regeneration of not just neuronal tissues, but other tissues as well.

Conclusion:

The results presented in this study indicate that MSC-EVs are endocytosed by retinal cells in a receptor-mediated, dose-dependent and saturable manner. The endocytosed EVs can protect retinal cells from cell death in simulated ischemic conditions *in vitro* and in retinal ischemia *in vivo*. Our findings on the involvement of HSPGs on the target cell surface in EV endocytosis and the binding of EVs to the vitreous serve as a basis for development of engineered EVs targeting these mechanisms for enhanced delivery and/or functionality. Furthermore, if these results can be extrapolated to other neuronal systems a common modality and a pathway for biomaterial based site-directed EV therapy may be established.

Data Availability

The raw/processed data required to reproduce these findings will be made available upon request.

Acknowledgements:

This research was supported by: National Institutes of Health (Bethesda, MD) grants RO1 EY010343 (Dr. Roth), R21 EY028690 (Dr. Roth), R56 DE023806 (Dr. Ravindran), R01 DE027404 (Dr. Ravindran), R01 EY026286 (Dr. Liu), P30 EY001792 to the Department of Ophthalmology and Visual Sciences at the University of Illinois at Chicago, UL1 TR002003 to the Center for Clinical and Translational Sciences at the University of Illinois at Chicago, a Catalyst Award from the Chicago Biomedical Consortium (Chicago, IL) to Dr. Roth, The Michael Reese Foundation (Chicago, IL) Pioneers Award to Dr. Roth, National Glaucoma Grant G2018168 from the Bright Focus Foundation (Clarksburg, MD) to Dr. Mathew, the Illinois Society for the Prevention of Blindness (Chicago, IL) to Ms. Sharma, a Medical Student Research Fellowship from the Craig Foundation (Chicago, IL) to Ms. Sharma, a Liberal Arts and Sciences Undergraduate Research Initiative Award and an Honors College Research Award to Mr. Chennakesavalu, and an unrestricted grant from Research to Prevent Blindness, Inc. (New York, NY) to the University of Illinois at Chicago Department of Ophthalmology and Visual Sciences.

Reference:

[1]. Duh EJ, Sun JK, Stitt AW, Diabetic retinopathy: current understanding, mechanisms, and treatment strategies, JCI insight 2(14) (2017).

[2]. Rivera JC, Dabouz R, Noueihed B, Omri S, Tahiri H, Chemtob S, Ischemic Retinopathies: Oxidative Stress and Inflammation, Oxidative medicine and cellular longevity 2017 (2017) 3940241. [PubMed: 29410732]

[3]. Yu B, Zhang X, Li X, Exosomes derived from mesenchymal stem cells, International journal of molecular sciences 15(3) (2014) 4142–57. [PubMed: 24608926]

[4]. Kim HJ, Park JS, Usage of Human Mesenchymal Stem Cells in Cell-based Therapy: Advantages and Disadvantages, Development & reproduction 21(1) (2017) 1–10. [PubMed: 28484739]

[5]. Roth S, Dreixler JC, Mathew B, Balyasnikova I, Mann JR, Boddapati V, Xue L, Lesniak MS, Hypoxic-Preconditioned Bone Marrow Stem Cell Medium Significantly Improves Outcome After Retinal Ischemia in RatsPreconditioned Stem Cells and Retinal Ischemia, Investigative ophthalmology & visual science 57(7) (2016) 3522–3532. [PubMed: 27367588]

[6]. Dreixler JC, Poston JN, Balyasnikova I, Shaikh AR, Lesniak MS, Roth S, Delayed administration of bone marrow mesenchymal stem cell conditioned medium significantly improves outcome after retinal ischemia in Rats, Investigative ophthalmology & visual science 55(6) (2014) 3785–3796. [PubMed: 24699381]

[7]. Mathew B, Poston JN, Dreixler JC, Torres L, Lopez J, Zelkha R, Balyasnikova I, Lesniak MS, Roth S, Bone-marrow mesenchymal stem-cell administration significantly improves outcome after retinal ischemia in rats, Graefe's archive for clinical and experimental ophthalmology = Albrecht von Graefes Archiv fur klinische und experimentelle Ophthalmologie 255(8) (2017) 1581–1592.

[8]. Johnson TV, Bull ND, Martin KR, Identification of barriers to retinal engraftment of transplanted stem cells, Investigative ophthalmology & visual science 51(2) (2010) 960–70. [PubMed: 19850833]

[9]. Yao Y, Huang J, Geng Y, Qian H, Wang F, Liu X, Shang M, Nie S, Liu N, Du X, Dong J, Ma C, Paracrine action of mesenchymal stem cells revealed by single cell gene profiling in infarcted murine hearts, PloS one 10(6) (2015) e0129164. [PubMed: 26043119]

[10]. Dai W, Hale SL, Kloner RA, Role of a paracrine action of mesenchymal stem cells in the improvement of left ventricular function after coronary artery occlusion in rats, Regenerative medicine 2(1) (2007) 63–8. [PubMed: 17465776]

[11]. Gnecchi M, Zhang Z, Ni A, Dzau VJ, Paracrine mechanisms in adult stem cell signaling and therapy, Circulation research 103(11) (2008) 1204–19. [PubMed: 19028920]

[12]. Huang C-C, Narayanan R, Alapati S, Ravindran S, Exosomes as biomimetic tools for stem cell differentiation: Applications in dental pulp tissue regeneration, Biomaterials.

[13]. Narayanan R, Huang CC, Ravindran S, Hijacking the Cellular Mail: Exosome Mediated Differentiation of Mesenchymal Stem Cells, Stem cells international 2016 (2016) 3808674. [PubMed: 26880957]

[14]. Wang X, Omar O, Vazirisani F, Thomsen P, Ekstrom K, Mesenchymal stem cell-derived exosomes have altered microRNA profiles and induce osteogenic differentiation depending on the stage of differentiation, PloS one 13(2) (2018) e0193059. [PubMed: 29447276]

[15]. Martins M, Ribeiro D, Martins A, Reis RL, Neves NM, Extracellular Vesicles Derived from Osteogenically Induced Human Bone Marrow Mesenchymal Stem Cells Can Modulate Lineage Commitment, Stem cell reports 6(3) (2016) 284–91. [PubMed: 26923821]

[16]. Zhang ZG, Chopp M, Exosomes in stroke pathogenesis and therapy, The Journal of clinical investigation 126(4) (2016) 1190–7. [PubMed: 27035810]

[17]. Goncalves MB, Malmqvist T, Clarke E, Hubens CJ, Grist J, Hobbs C, Trigo D, Risling M, Angeria M, Damberg P, Carlstedt TP, Corcoran JP, Neuronal RARbeta Signaling Modulates PTEN Activity Directly in Neurons and via Exosome Transfer in Astrocytes to Prevent Glial Scar Formation and Induce Spinal Cord Regeneration, The Journal of neuroscience: the official journal of the Society for Neuroscience 35(47) (2015) 15731–45. [PubMed: 26609164]

[18]. Zhang B, Yin Y, Lai RC, Lim SK, Immunotherapeutic potential of extracellular vesicles, Frontiers in immunology 5 (2014) 518. [PubMed: 25374570]

[19]. Doeppner TR, Herz J, Gorgens A, Schlechter J, Ludwig AK, Radtke S, de Miroschedji K, Horn PA, Giebel B, Hermann DM, Extracellular Vesicles Improve Post-Stroke Neuroregeneration and Prevent Postischemic Immunosuppression, Stem cells translational medicine 4(10) (2015) 1131–43. [PubMed: 26339036]

[20]. Khan M, Nickoloff E, Abramova T, Johnson J, Verma SK, Krishnamurthy P, Mackie AR, Vaughan E, Garikipati VN, Benedict C, Ramirez V, Lambers E, Ito A, Gao E, Misener S, Luongo T, Elrod J, Qin G, Houser SR, Koch WJ, Kishore R, Embryonic stem cell-derived exosomes promote endogenous repair mechanisms and enhance cardiac function following myocardial infarction, Circulation research 117(1) (2015) 52–64. [PubMed: 25904597]

[21]. Zappulli V, Friis KP, Fitzpatrick Z, Maguire CA, Breakefield XO, Extracellular vesicles and intercellular communication within the nervous system, The Journal of clinical investigation 126(4) (2016) 1198–207. [PubMed: 27035811]

[22]. Beninson LA, Fleshner M, Exosomes: an emerging factor in stress-induced immunomodulation, Seminars in immunology 26(5) (2014) 394–401. [PubMed: 24405946]

[23]. Pitt JM, Kroemer G, Zitvogel L, Extracellular vesicles: masters of intercellular communication and potential clinical interventions, The Journal of clinical investigation 126(4) (2016) 1139–43. [PubMed: 27035805]

[24]. Mulcahy LA, Pink RC, Carter DR, Routes and mechanisms of extracellular vesicle uptake, Journal of extracellular vesicles 3 (2014).

[25]. Morelli AE, Larregina AT, Shufesky WJ, Sullivan ML, Stolz DB, Papworth GD, Zahorchak AF, Logar AJ, Wang Z, Watkins SC, Falo LD, Jr., Thomson AW, Endocytosis, intracellular sorting, and processing of exosomes by dendritic cells, Blood 104(10) (2004) 3257–66. [PubMed: 15284116]

[26]. Christianson HC, Svensson KJ, van Kuppevelt TH, Li JP, Belting M, Cancer cell exosomes depend on cell-surface heparan sulfate proteoglycans for their internalization and functional activity, Proceedings of the National Academy of Sciences of the United States of America 110(43) (2013) 17380–5. [PubMed: 24101524]

[27]. Chen L, Brigstock DR, Integrins and heparan sulfate proteoglycans on hepatic stellate cells (HSC) are novel receptors for HSC-derived exosomes, FEBS Lett 590(23) (2016) 4263–4274. [PubMed: 27714787]

[28]. Costa Verdera H, Gitz-Francois JJ, Schiffelers RM, Vader P, Cellular uptake of extracellular vesicles is mediated by clathrin-independent endocytosis and macropinocytosis, Journal of controlled release: official journal of the Controlled Release Society 266 (2017) 100–108.

[29]. Cheung CY, Ikram MK, Chen C, Wong TY, Imaging retina to study dementia and stroke, Progress in retinal and eye research 57 (2017) 89–107. [PubMed: 28057562]

[30]. Avery RL, Bakri SJ, Blumenkranz MS, Brucker AJ, Cunningham ET, Jr., D'Amico DJ, Dugel PU, Flynn HW, Jr., Freund KB, Haller JA, Jumper JM, Liebmann JM, McCannel CA, Mieler WF, Ta CN, Williams GA, Intravitreal injection technique and monitoring: updated guidelines of an expert panel, Retina 34 Suppl 12 (2014) S1–s18. [PubMed: 25489719]

[31]. Le Goff MM, Bishop PN, Adult vitreous structure and postnatal changes, Eye (London, England) 22(10) (2008) 1214–22.

[32]. Mead B, Amaral J, Tomarev S, Mesenchymal Stem Cell-Derived Small Extracellular Vesicles Promote Neuroprotection in Rodent Models of Glaucoma, Investigative ophthalmology & visual science 59(2) (2018) 702–714. [PubMed: 29392316]

[33]. Mead B, Tomarev S, Bone Marrow-Derived Mesenchymal Stem Cells-Derived Exosomes Promote Survival of Retinal Ganglion Cells Through miRNA-Dependent Mechanisms, Stem cells translational medicine (2017).

[34]. Huang CC, Narayanan R, Alapati S, Ravindran S, Exosomes as biomimetic tools for stem cell differentiation: Applications in dental pulp tissue regeneration, Biomaterials 111 (2016) 103–115. [PubMed: 27728810]

[35]. McNicholas K, Michael MZ, Immuno-characterization of Exosomes Using Nanoparticle Tracking Analysis, Methods in molecular biology (Clifton, N.J.) 1545 (2017) 35–42.

[36]. Szatanek R, Baj-Krzyworzeka M, Zimoch J, Lekka M, Siedlar M, Baran J, The Methods of Choice for Extracellular Vesicles (EVs) Characterization, International journal of molecular sciences 18(6) (2017).

[37]. Keerthikumar S, Chisanga D, Ariyaratne D, Al Saffar H, Anand S, Zhao K, Samuel M, Pathan M, Jois M, Chilamkurti N, Gangoda L, Mathivanan S, ExoCarta: A Web-Based Compendium of Exosomal Cargo, Journal of Molecular Biology 428(4) (2016) 688–692. [PubMed: 26434508]

[38]. Gutkin A, Uziel O, Beery E, Nordenberg J, Pinchasi M, Goldvaser H, Henick S, Goldberg M, Lahav M, Tumor cells derived exosomes contain hTERT mRNA and transform nonmalignant fibroblasts into telomerase positive cells, Oncotarget 7(37) (2016) 59173–59188. [PubMed: 27385095]

[39]. Kong D, Gong L, Arnold E, Shanmugam S, Fort PE, Gardner TW, Abcouwer SF, Insulin-like growth factor 1 rescues R28 retinal neurons from apoptotic death through ERK-mediated BimEL phosphorylation independent of Akt, Experimental eye research 151 (2016) 82–95. [PubMed: 27511131]

[40]. Seigel GM, Review: R28 retinal precursor cells: the first 20 years, Molecular vision 20 (2014) 301–6. [PubMed: 24644404]

[41]. Hu X, Dai Y, Sun X, Parkin overexpression protects retinal ganglion cells against glutamate excitotoxicity, Molecular vision 23 (2017) 447–456. [PubMed: 28761318]

[42]. Morte MI, Carreira BP, Machado V, Carmo A, Nunes-Correia I, Carvalho CM, Araujo IM, Evaluation of proliferation of neural stem cells in vitro and in vivo, Current protocols in stem cell biology Chapter 2 (2013) Unit 2D.14.

[43]. Clarke ST, Calderon V, Bradford JA, Click Chemistry for Analysis of Cell Proliferation in Flow Cytometry, Current protocols in cytometry 82 (2017) 7.49.1–7.49.30.

[44]. Roth S, Shaikh AR, Hennelly MM, Li Q, Bindokas V, Graham CE, Mitogen-activated protein kinases and retinal ischemia, Investigative ophthalmology & visual science 44 (2003) 5383–95. [PubMed: 14638742]

[45]. Roth S, Dreixler JC, Shaikh AR, Lee KH, Bindokas V, Mitochondrial potassium ATP channels and retinal ischemic preconditioning, Investigative ophthalmology & visual science 47 (2006) 2114–24. [PubMed: 16639023]

[46]. Dreixler JC, Shaikh AR, Shenoy SK, Shen Y, Roth S, Protein kinase C subtypes and retinal ischemic preconditioning, Experimental eye research 87 (2008) 300–11. [PubMed: 18722601]

[47]. Dreixler J, Shaikh A, Alexander M, Savoie B, Roth S, Post-ischemic conditioning in the rat retina is dependent upon ischemia duration and is not additive with ischemic preconditioning, Experimental eye research 91 (2010) 844–852. [PubMed: 20599964]

[48]. Dreixler JC, Bratton A, Du E, Shaikh AR, Marcet MM, Roth S, Mitogen activated protein kinase phosphatase-1 (MKP-1) in retinal ischemic preconditioning Experimental eye research 93 (2011) 340–9. [PubMed: 21094639]

[49]. Dreixler JC, Poston JN, Shaikh AR, Alexander M, Tupper KY, Marcet MM, Bernaudin M, Roth S, Delayed post-ischemic conditioning significantly improves the outcome after retinal ischemia, Experimental eye research 92(6) (2011) 521–7. [PubMed: 21501608]

[50]. Dreixler JC, Sampat A, Shaikh AR, Alexander M, Marcet MM, Roth S, Protein kinase B (Akt) and mitogen-activated protein kinase p38alpha in retinal ischemic post-conditioning, J Mol Neurosci 45(2) (2011) 309–20. [PubMed: 21573888]

[51]. Fang IM, Yang CM, Yang CH, Chitosan oligosaccharides prevented retinal ischemia and reperfusion injury via reduced oxidative stress and inflammation in rats, Experimental eye research 130 (2015) 38–50. [PubMed: 25479043]

[52]. Roth S, Dreixler JC, Newman NJ, Haemodilution and head-down tilting induce functional injury in the rat optic nerve: A model for peri-operative ischemic optic neuropathy, Eur J Anaesthesiology 2018 May 15. doi: 10.1097/EJA.0000000000000829. [Epub ahead of print] (2018).

[53]. Feng L, Puyang Z, Chen H, Liang P, Troy JB, Liu X, Overexpression of Brain-Derived Neurotrophic Factor Protects Large Retinal Ganglion Cells After Optic Nerve Crush in Mice, eNeuro 4(1) (2017) ENEURO.0331–16.2016.

[54]. Hu P, Hunt NH, Arfuso F, Shaw LC, Uddin MN, Zhu M, Devasahayam R, Adamson SJ, Benson VL, Chan-Ling T, Grant MB, Increased Indoleamine 2,3-Dioxygenase and Quinolinic Acid Expression in Microglia and Muller Cells of Diabetic Human and Rodent Retina, Investigative ophthalmology & visual science 58(12) (2017) 5043–5055. [PubMed: 28980000]

[55]. Nadal-Nicolas FM, Jimenez-Lopez M, Sobrado-Calvo P, Nieto-Lopez L, Canovas-Martinez I, Salinas-Navarro M, Vidal-Sanz M, Agudo M, Brn3a as a marker of retinal ganglion cells: qualitative and quantitative time course studies in naive and optic nerve-injured retinas, Investigative ophthalmology & visual science 50(8) (2009) 3860–8. [PubMed: 19264888]

[56]. Mead B, Thompson A, Scheven BA, Logan A, Berry M, Leadbeater W, Comparative evaluation of methods for estimating retinal ganglion cell loss in retinal sections and wholemounts, PloS one 9(10) (2014) e110612. [PubMed: 25343338]

[57]. Singh M, Savitz SI, Hoque R, Rosenbaum PS, Roth S, Rosenbaum DM, Cell-specific caspase expression by different neuronal phenotypes in transient retinal ischemia, Journal of neurochemistry 77 (2001) 466–475. [PubMed: 11299309]

[58]. Zhang C, Rosenbaum DM, Shaikh AR, Q L, Rosenbaum PS, Pelham DJ, Roth S, Ischemic preconditioning attenuates apoptosis following retinal ischemia in rats, Investigative ophthalmology & visual science 43 (2002) 3059–3066. [PubMed: 12202530]

[59]. Phinney DG, Pittenger MF, Concise Review: MSC-Derived Exosomes for Cell-Free Therapy, Stem Cells 35(4) (2017) 851–858. [PubMed: 28294454]

[60]. Lotvall J, Hill AF, Hochberg F, Buzas EI, Di Vizio D, Gardiner C, Gho YS, Kurochkin IV, Mathivanan S, Quesenberry P, Sahoo S, Tahara H, Wauben MH, Witwer KW, Thery C, Minimal experimental requirements for definition of extracellular vesicles and their functions: a position statement from the International Society for Extracellular Vesicles, Journal of extracellular vesicles 3 (2014) 26913. [PubMed: 25536934]

[61]. Svensson KJ, Christianson HC, Wittrup A, Bourseau-Guilmain E, Lindqvist E, Svensson LM, Morgelin M, Belting M, Exosome uptake depends on ERK1/2-heat shock protein 27 signaling and lipid Raft-mediated endocytosis negatively regulated by caveolin-1, The Journal of biological chemistry 288(24) (2013) 17713–24. [PubMed: 23653359]

[62]. Mahammad S, Parmryd I, Cholesterol depletion using methyl-beta-cyclodextrin, Methods in molecular biology (Clifton, N.J.) 1232 (2015) 91–102.

[63]. Medvedeva YV, Ji SG, Yin HZ, Weiss JH, Differential Vulnerability of CA1 versus CA3 Pyramidal Neurons After Ischemia: Possible Relationship to Sources of Zn2+ Accumulation and Its Entry into and Prolonged Effects on Mitochondria, The Journal of neuroscience: the official journal of the Society for Neuroscience 37(3) (2017) 726–737.

[64]. Tan LE, Orilla W, Hughes PM, Tsai S, Burke JA, Wilson CG, Effects of vitreous liquefaction on the intravitreal distribution of sodium fluorescein, fluorescein dextran, and fluorescent microparticles, Investigative ophthalmology & visual science 52(2) (2011) 1111–8. [PubMed: 20881289]

[65]. Kowal EJK, Ter-Ovanesyan D, Regev A, Church GM, Extracellular Vesicle Isolation and Analysis by Western Blotting, Methods in molecular biology (Clifton, N.J.) 1660 (2017) 143–152.

[66]. Park SS, Moisseiev E, Bauer G, Anderson JD, Grant MB, Zam A, Zawadzki RJ, Werner JS, Nolta JA, Advances in bone marrow stem cell therapy for retinal dysfunction, Progress in retinal and eye research 56 (2017) 148–165. [PubMed: 27784628]

[67]. Chen J, Chopp M, Exosome Therapy for Stroke, Stroke 49(5) (2018) 1083–1090. [PubMed: 29669873]

[68]. Li C, Liu DR, Li GG, Wang HH, Li XW, Zhang W, Wu YL, Chen L, CD97 promotes gastric cancer cell proliferation and invasion through exosome-mediated MAPK signaling pathway, World journal of gastroenterology 21(20) (2015) 6215–28. [PubMed: 26034356]

[69]. Alcayaga-Miranda F, Varas-Godoy M, Khoury M, Harnessing the Angiogenic Potential of Stem Cell-Derived Exosomes for Vascular Regeneration, Stem cells international 2016 (2016) 11.

[70]. Taylor-Walker G, Lynn SA, Keeling E, Munday R, Johnston DA, Page A, Scott JA, Goverdhan S, Lotery AJ, Ratnayaka JA, The Alzheimer's-related amyloid beta peptide is internalised by R28 neuroretinal cells and disrupts the microtubule associated protein 2 (MAP-2), Experimental eye research 153 (2016) 110–121. [PubMed: 27751744]

[71]. Gump JM, Thorburn A, Sorting cells for basal and induced autophagic flux by quantitative ratiometric flow cytometry, Autophagy 10(7) (2014) 1327–1334. [PubMed: 24915460]

[72]. Kaushik S, Cuervo AM, Methods to monitor chaperone-mediated autophagy, Methods Enzymol 452 (2009) 297–324. [PubMed: 19200890]

[73]. Rosenbaum DM, Rosenbaum PS, Gupta H, Singh M, Aggarwal A, Hall DH, Roth S, Kessler JA, The role of the p53 protein in the selective vulnerability of the inner retina to transient ischemia, Investigative ophthalmology & visual science 39(11) (1998) 2132–2139. [PubMed: 9761292]

[74]. Joerger-Messerli MS, Oppliger B, Spinelli M, Thomi G, di Salvo I, Schneider P, Schoeberlein A, Extracellular Vesicles Derived from Wharton's Jelly Mesenchymal Stem Cells Prevent and Resolve Programmed Cell Death Mediated by Perinatal Hypoxia-Ischemia in Neuronal Cells, Cell Transplant 27(1) (2018) 168–180. [PubMed: 29562785]

[75]. Shigemoto-Kuroda T, Oh JY, Kim DK, Jeong HJ, Park SY, Lee HJ, Park JW, Kim TW, An SY, Prockop DJ, Lee RH, MSC-derived Extracellular Vesicles Attenuate Immune Responses in Two Autoimmune Murine Models: Type 1 Diabetes and Uveoretinitis, Stem cell reports 8(5) (2017) 1214–1225. [PubMed: 28494937]

[76]. Subirada PV, Paz MC, Ridano ME, Lorenc VE, Vaglienti MV, Barcelona PF, Luna JD, Sanchez MC, A journey into the retina: Muller glia commanding survival and death, The European journal of neuroscience (2018).

[77]. Arroba AI, Valverde AM, Modulation of microglia in the retina: new insights into diabetic retinopathy, Acta diabetologica 54(6) (2017) 527–533. [PubMed: 28349217]

[78]. Wang JW, Chen SD, Zhang XL, Jonas JB, Retinal Microglia in Glaucoma, Journal of glaucoma 25(5) (2016) 459–65. [PubMed: 25646715]

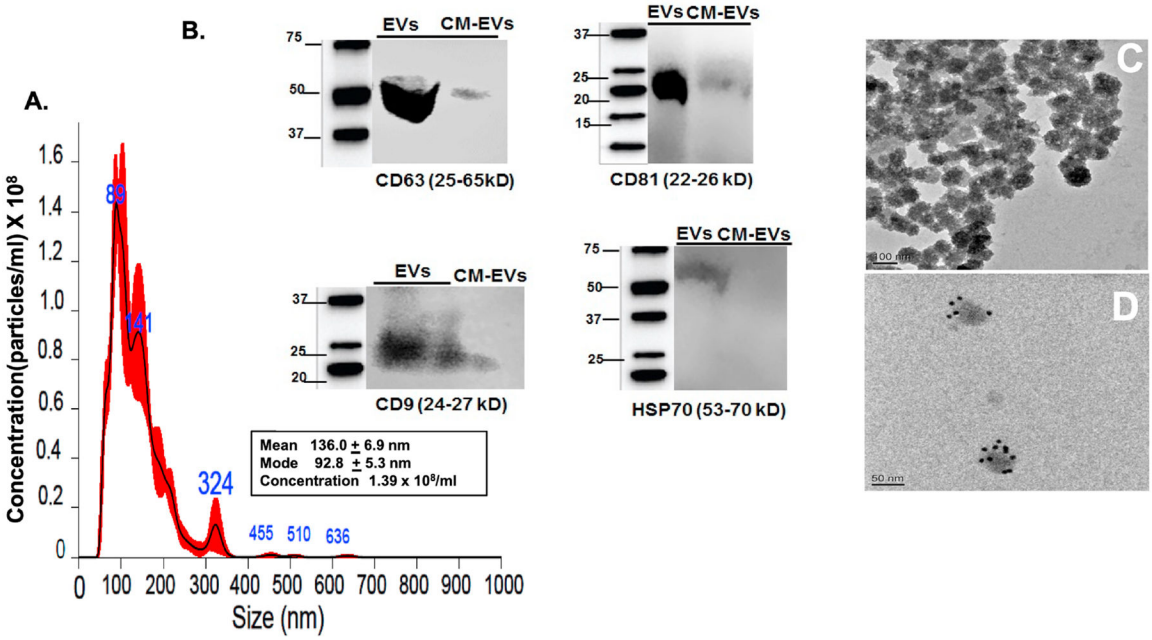

Fig 1. Characterization of MSC derived EVs.

(**A**) Nanoparticle Tracking Analysis (NTA) histogram demonstrating MSC-EVs' size distribution after isolation using centrifugation and EV Exo-quick Isolation Reagent (see Methods for details). In the insert, mean and mode for particle size are displayed along with concentration. MSC-EVs showed a modal size of 93 nm, peaks at 89 and 141 nm (see Results for explanation), and the presence of few large vesicles (shown as larger peaks at higher diameters) indicating that the majority of the MSC-EVs are likely exosomes. (**B**) Western blot illustrating the characteristic surface markers of exosomes, CD63, CD9, CD81, and HSP70α, present in MSC-EV preparations, but not in MSC-conditioned medium (CM) depleted of EVs. Molecular weight markers are on left of each blot. (**C**) Transmission electron microscopic (TEM) image of cup-shaped MSC-EVs isolated from MSCs with diameters of approximately 100 nm, consistent with exosomal size. (D) Immunogold labeling of MSC-EVs with CD63 antibody to exosome surface markers, again demonstrating that the MSC-EVs are mainly exosomes. Scale bars are on lower left of Figs 1C and 1D.

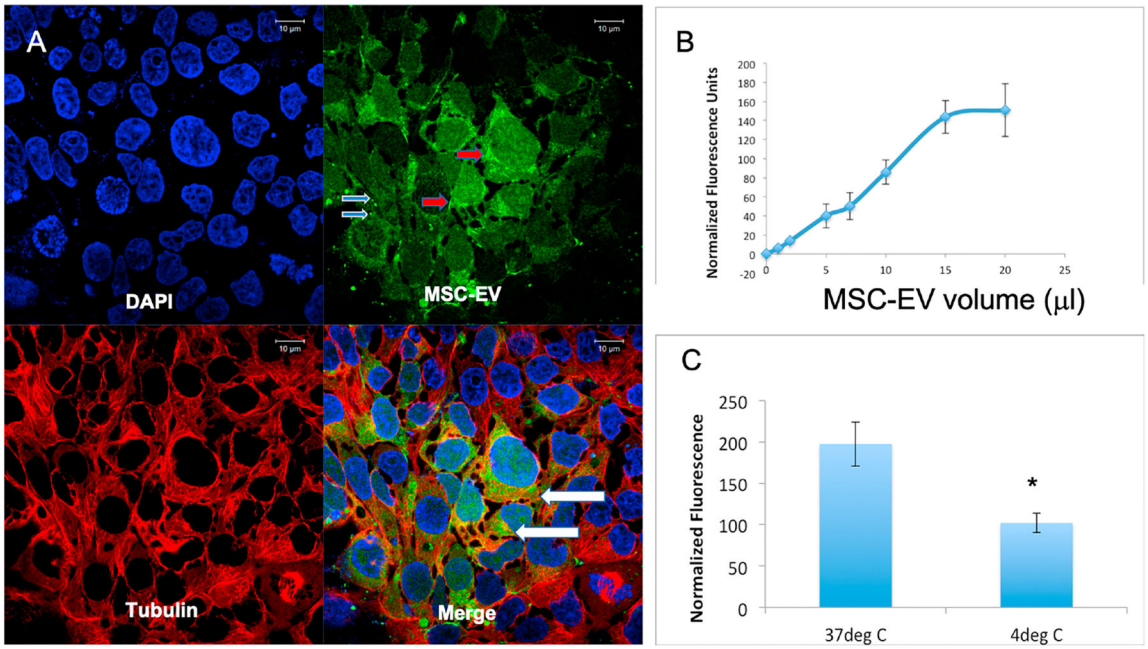

Fig 2.

Endocytosis of MSC-EVs by R28 cells: (**A**) Representative confocal micrograph demonstrating endocytosis of fluorescently labeled EVs (green) by R28 cells. The cells were counter-stained with primary antibody to tubulin (cytoskeleton, red), and with DAPI to stain the nuclei (blue). Clockwise from top left are: DAPI (blue), MSC-EVs (green), composite of DAPI, MSCEVs, and tubulin (red). The image on top right of **2A** demonstrates green punctae of MSC-EVs (light blue arrows) and denser concentrations of MSC-EVs (red arrows), and there is co-localization of MSC-EVs and tubulin within the cytoplasm of the cells (white arrows in lower right, composite panel of **2A**). Scale bars are on the top of each panel. (**B**) Graph indicates a dose-dependent and saturable endocytosis of fluorescently labeled MSC-EVs. X-axis is volume of MSC-EVs and Y-axis indicates mean normalized fluorescence units. (**C**) Quantitative fluorescence measurements of MSC-EV endocytosis at 37°C and 4°C showing a decrease in endocytosis at lower temperature. Temperature is on X-axis, and Y-axis is mean normalized fluorescence units. The data represented in **2B** and **2C** are the mean of 6 individual experiments, and error bars indicate SD. * in Fig 2C represents statistical significance with respect to control (normothermia, $P < 0.01$).

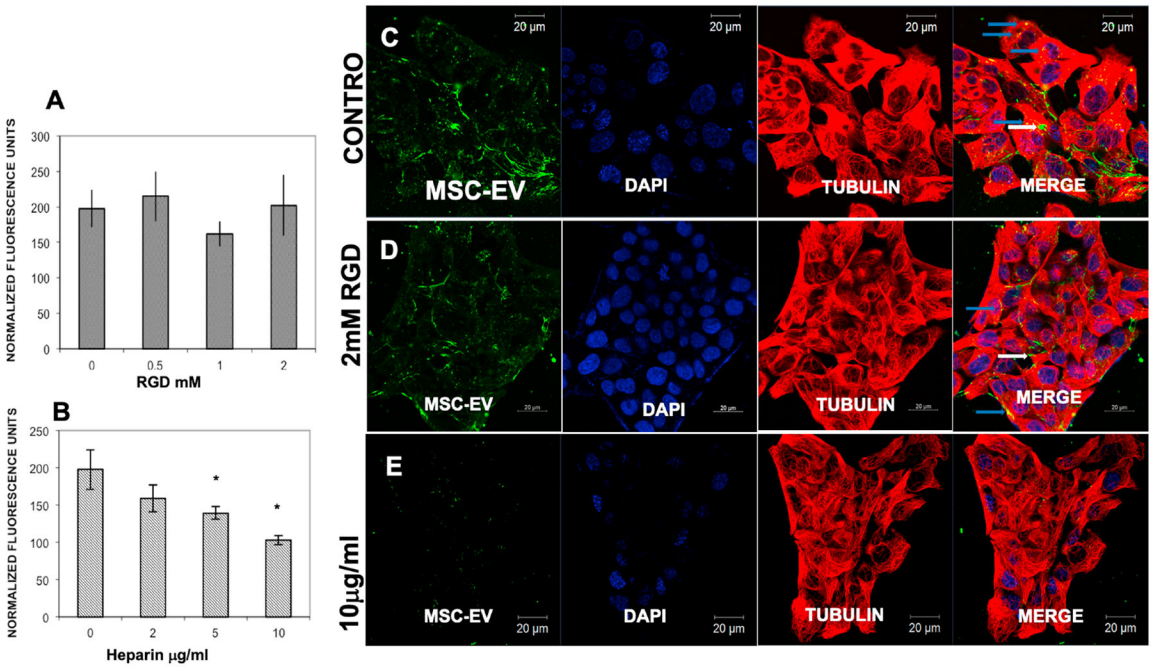

Fig 3. Heparan sulfate proteoglycans (HSPGs), but not integrins, are involved in endocytosis of MSC-EVs by R28 cells:

(**A**) Increasing doses of RGD peptide to block cell surface integrins did not alter endocytosis of fluorescently labeled MSC-EVs. Y-axis is mean normalized fluorescence units ± SD; the X-axis is dose of RGD in mM. No statistical significance was observed (n = 6 experiments). (**B**) Dose-dependent reduction of fluorescently labeled MSC-EV endocytosis after heparin pre-treatment to block HSPGs. Data on Y-axis is mean normalized fluorescence units ± SD; the X-axis is dose of heparin in µg/ml. * = $P < 0.05$ compared to vehicle (heparin = "0"), n = 6 experiments. (**C**) Representative confocal micrograph showing endocytosis of fluorescently labeled MSC-EVs by R28 cells treated with PBS vehicle (control). (**D**) Representative confocal micrograph showing no reduction in endocytosis of MSC-EVs after pre-incubation with RGD to block integrins (RGD = "0" is PBS vehicle alone). (**E**) Representative confocal micrograph showing reduction in endocytosis of MSC-EVs after they were pre-incubated with heparin to block HSPGs. (For **C, D, and E**, from left to right are shown MSCEVs (green), DAPI to stain the cell nuclei (blue), anti-tubulin to stain cytoskeleton (red), and composite of MSC-EVs, DAPI, and tubulin on the far right. Endocytosis can be seen in **C and D**, in the far right panels, where green MSC-EVs are visible inside cells (white arrows), as well as overlapping with tubulin (blue arrows). Scale bars appear on top or bottom of each panel.

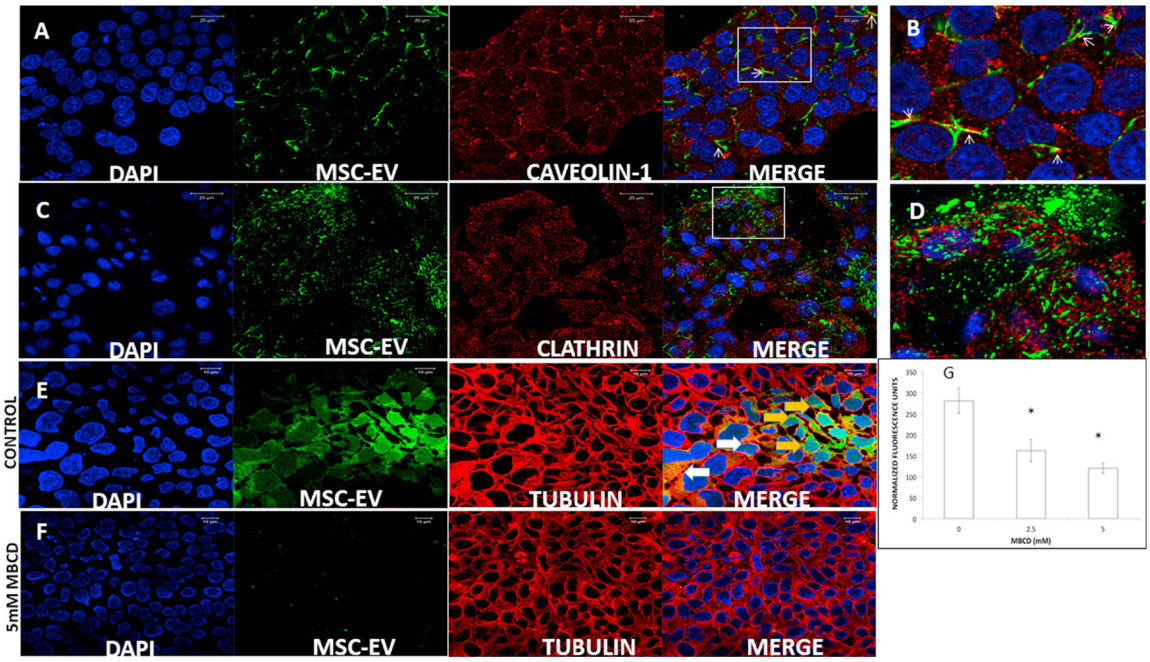

Fig 4. Involvement of the caveolar pathway in MSC-EV endocytosis by R28 cells:

(**A**) Representative confocal images showing endocytosed fluorescently labeled MSC-EVs (green) co-localized with anti-caveolin 1 (red). From left to right are DAPI (blue), MSC-EVs (green), cave-olin-1 (red), and merged. (**B**) Magnified area of box in **A**. White arrowheads point to regions of co-localization of caveolin-1 and MSC-EVs, as indicated by overlap of red and green to appear as yellow. (**C**) Representative confocal images of endocytosed MSC-EVs counterstained with anti-clathrin (red). From left to right are DAPI (blue), MSC-EVs (green), clathrin (red), and merged. (**D**) Magnified area of box in **C**. Note that in contrast to **4A-B**, there is no co-localization of MSC-EVs and clathrin in **C** and in **D**. (**E**) Representative confocal images showing endocytosed fluorescently labeled MSC-EVs (green) in R28 cells. From left to right are DAPI (blue), MSC-EVs (green), anti-tubulin (red), and merged. MSC-EVs are visible inside the cells in the far right merged panel (green, shown by orange arrows), or yellow/orange, where tubulin (red) and MSC-EVs (green), co-localize (shown by white arrows). (**F**) Representative confocal images showing endocytosed fluorescently labeled MSC-EVs (green) in R28 cells after pre-treatment with methyl-β-cyclodextrin (MBCD) to disrupt R28 cell membrane cholesterol. From left to right are DAPI (blue), MSC-EVs (green), tubulin (red), and merged. **(G**) Quantitation of MBCD effect on endocytosis of MSC-EVs into R28 cells. There was a significant dose dependent reduction in MSC-EV uptake with increasing doses of MBCD. Data on the Y-axis is mean normalized fluorescence units ± SD; the X-axis is dose of MBCD in mM. * = $P < 0.05$ compared to control, n = 6 experiments.

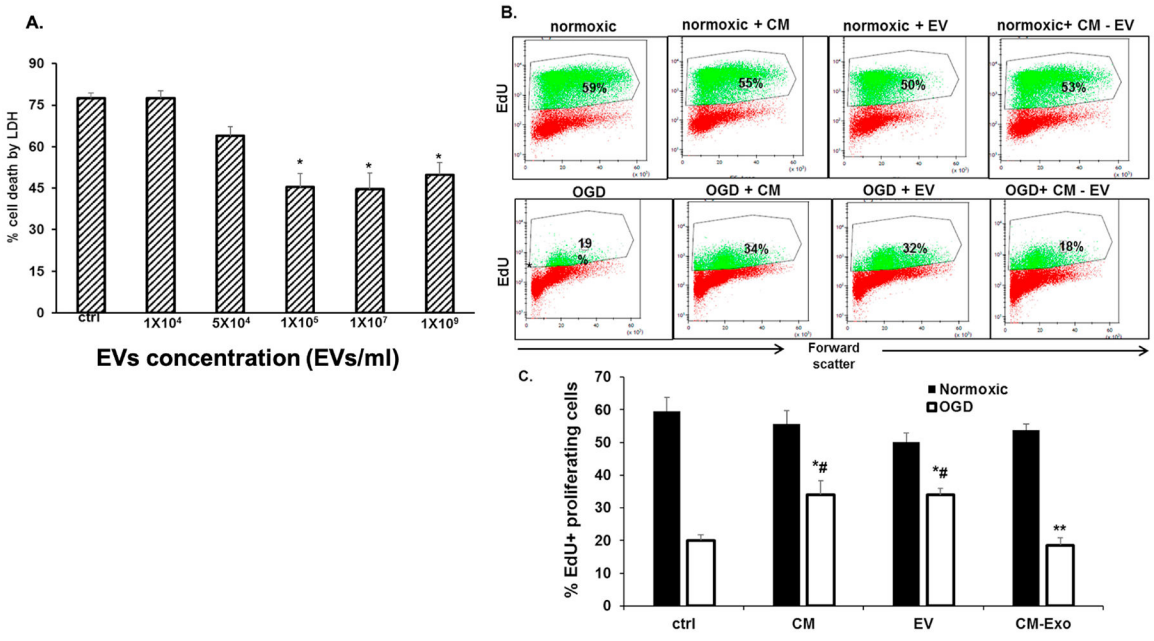

Fig 5. EVs protect retinal cells from OGD-induced cell death:

(A) Dose dependent effect of MSC-EVs on oxygen glucose deprivation (OGD) induced cytotoxicity of R28 cells as measured by lactate dehydrogenase (LDH) assay. Note the decrease in cell death from OGD with increasing dosage of MSC-EVs with saturation at 10^5 EVs/ml. In (**A**) data is presented as percentage cytotoxicity on Y-axis (% cell death, LDH, mean ± SD), and X-axis is concentration of MSCEVs in particles/ml. n = 6 experiments * = P < 0.05 vs OGD alone. (**B**) Representative flow cytometry results for the presence of EdU-positive cells after OGD with and without EVs. The percentages within the graphs in bold indicate the % of proliferating cells. Conditioned medium (CM) without EVs (CM-Exo), and PBS (ctrl) were controls. Exo = EVs. (**C**) Graphical representation of results in (**B**). Y-axis is % EdU-positive cells (mean ± SD). N = 4 experiments, * = p < 0.05 normoxia vs OGD, # = p < 0.05 vs control ("ctrl", OGD + PBS). Both CM and Exo prevented the loss of proliferation in cells subjected to OGD, while CM-Exo showed no effect. Although there was a small decrease in proliferation in normoxic cells treated with EVs, there was no significant difference from controls.

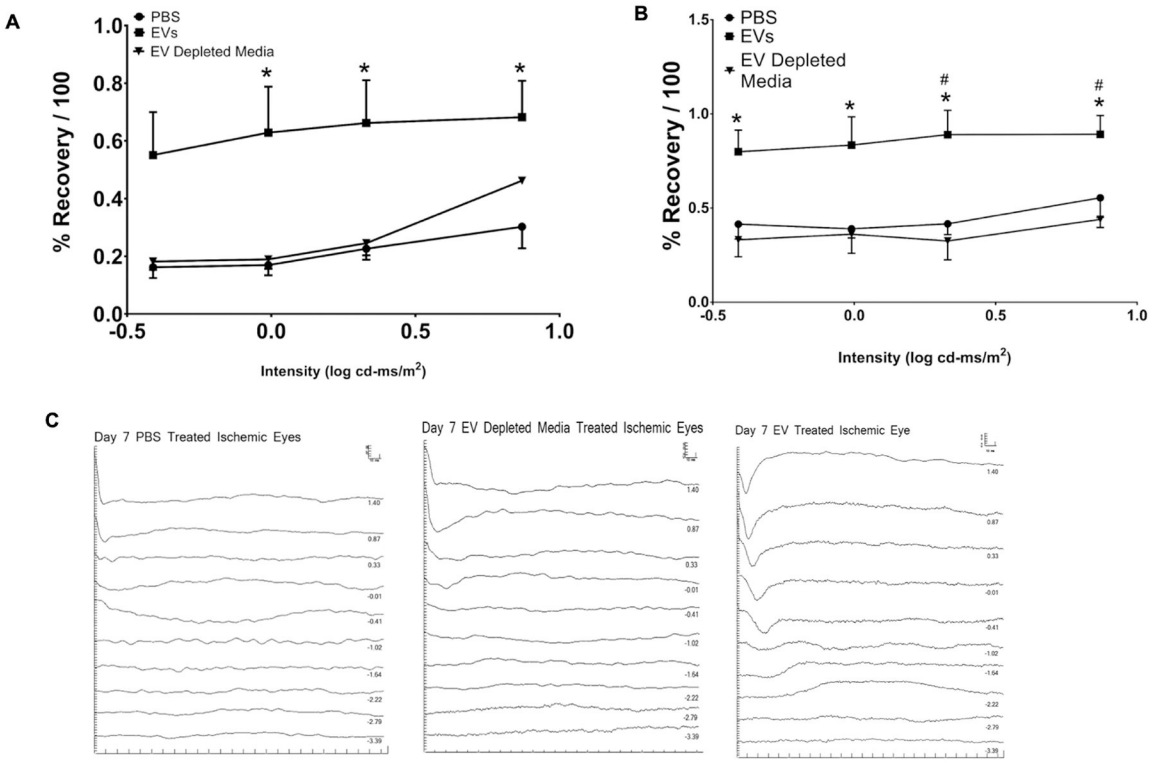

Fig 6. MSC-EVs enhance functional recovery after retinal ischemia *in vivo*.

Stimulus intensity plots of a-(**A**) and b-waves (**B**) were measured at baseline and at 8 days post ischemia. MSCEVs, PBS, or MSC medium depleted of EVs (EV depleted medium) were injected 24 h after ischemia into the vitreous humor of both eyes (right eye was ischemic and left eye was non ischemic control), as described in the methods section. (**C**) Representative ERG traces from ischemic retinae injected with PBS, MSC-EVs and medium depleted of EVs respectively; for brevity, only one set of representative traces, from ischemic eyes, per group is shown. The scale bars for amplitude (Y-axis, μV) and latency (X-axis, ms) appear in the top right of each representative ERG panel. N = 11–13 rats, for MSC-EVs or PBS; N = 6 for MSC-EV depleted medium. * = $P < 0.05$ for ischemic + MSC-EVs *vs* ischemic + PBS, # = $P < 0.05$ for medium depleted of MSC-EVs + ischemic *vs* MSC-EVs + ischemic.

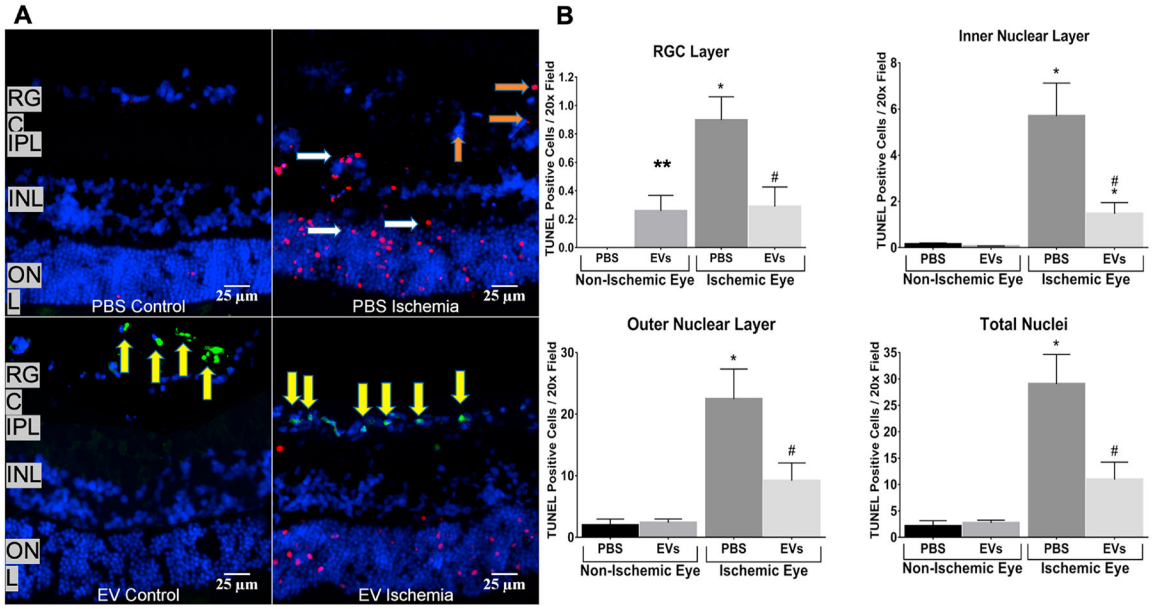

Fig 7. MSC-EVs attenuated ischemia-induced apoptosis (TUNEL, terminal deoxynucleotidyl transferase-mediated dUTP nick end labeling assay) in ischemic retinae *in vivo*.

(**A**) Representative immuno-histochemical images of TUNEL in retinal cryosections (7 µm) demonstrating MSC-EV-mediated reduction in TUNEL cells in ischemic retina compared to PBS injected ischemic. Red = TUNEL; Blue = DAPI, Green = fluorescently labeled MSC-EVs. In these experiments, the retinal cryosections were taken from retinae at 24 h after intravitreal injection of MSC-EVs or PBS, which was 48 h after ischemia. TUNEL cells are seen in the RGC layer (orange arrows), and in the inner (INL) and outer nuclear layers (ONL). (white arrows). IPL = inner plexiform layer. Note that aggregates of green MSC-EVs (yellow arrows) are present in the retinal ganglion cell (RGC) layer in EV ischemia (bottom right panel), and in the vitreous in EV control (bottom left panel). (**B**) Graphical representation of TUNEL cells in retinal ganglion cell layer, inner nuclear layer, outer nuclear layer, and total nuclei in retina, with data shown on Y-axis as TUNEL cells/20× field, mean ± SD. TUNEL was counted in all four groups (PBS control, MSC-EV control, PBS + ischemia and MSC-EVs + ischemia) by blinded observers. MSCEVs attenuated TUNEL in ischemic retinae, and there was no significant increase in TUNEL in normal eyes injected with MSC-EVs (“EV control”) except in the RGC layer. N = 4 rats per group; * = $P < 0.05$ for PBS non-ischemic vs PBS ischemic, or MSC-EV non ischemic vs MSCEV ischemic; # = $P < 0.05$ for PBS ischemic vs MSC-EV ischemic. ** = $P < 0.05$ for MSC-EV non-ischemic vs PBS non-ischemic.

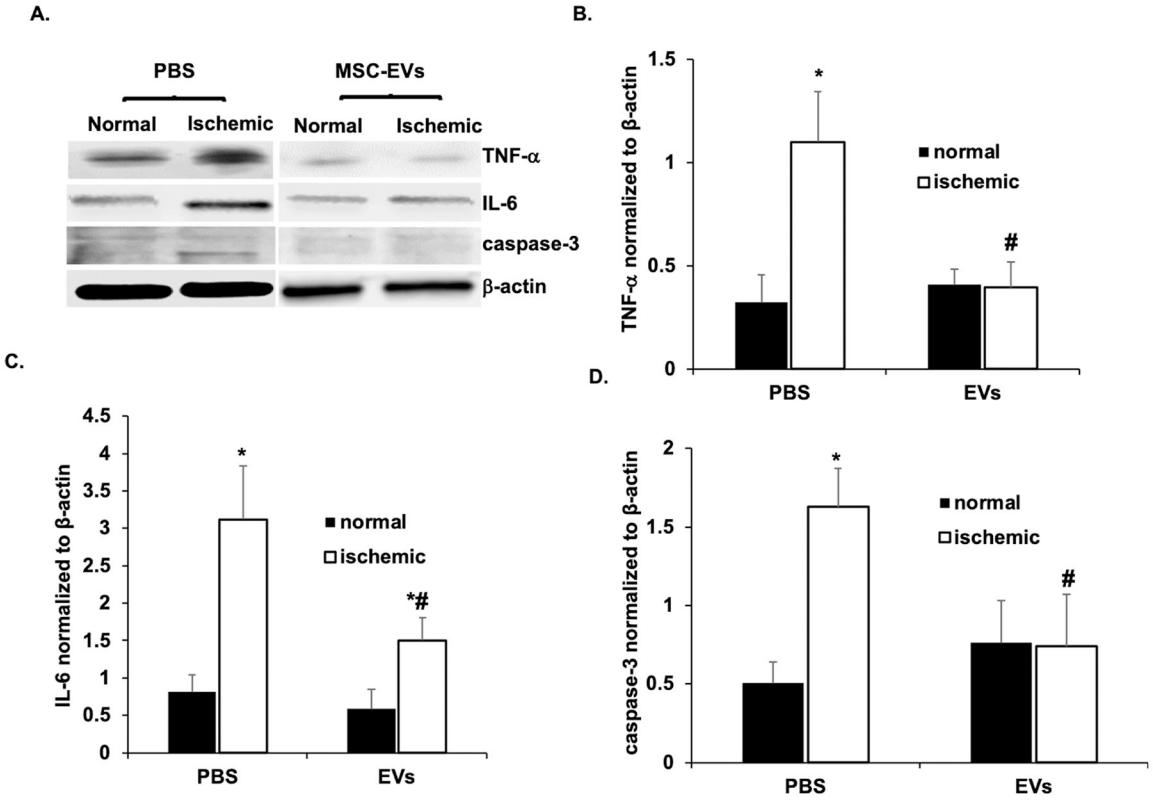

Fig 8. MSC-EVs attenuated neuro-inflammation and caspase 3 activation after retinal ischemia *in vivo*:

(**A**) Representative Western blots for TNFα, IL-6 and cleaved caspase 3. β-Actin was used as the loading control. (**B, C and D**) are quantitative bar graphs of Western blots illustrating the significant MSC-EV-mediated amelioration of ischemia-induced increases in levels of inflammatory mediumtors (IL-6, TNFα), and apoptosis (cleaved caspase 3) in rats injected with intravitreal MSC-EVs 24 h after ischemia. There was no significant change in levels of IL-6, TNFα, or caspase 3 in MSC-EV injected normal eyes compared to PBS injected normal eyes. Retinal samples were collected 48 h after ischemia, which was 24 h after MSC-EV or PBS injection. N = 10 rats per group, * = $P < 0.05$ control non-ischemic vs ischemic, # = $p < 0.05$ PBS + ischemic vs MSC-EV + ischemic.

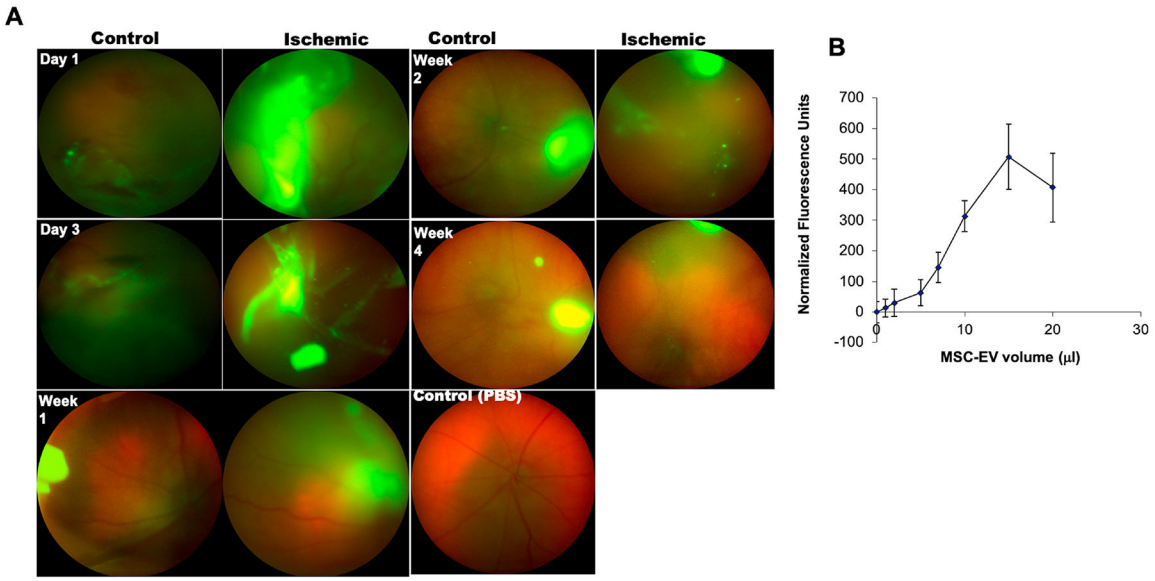

Fig 9. *In vivo* live imaging of intra-vitreally injected green fluorescent MSC-EVs.

(**A**) Up-take of MSC-EVs into vitreous and retina of normal and ischemic eyes was imaged in real time by *in vivo* fundus imaging for a time course of four weeks (days 1 and 3, weeks 1, 2 and 4), using a Phoenix Micron IV (See Methods for more details). The control non-ischemic eyes are on the left and the ischemic on the right in each of the two columns in (**A**). Fluorescent MSC-EVs were present for up to 4 weeks after injection into the vitreous humor. Concentration of the MSC-EVs at the sites of injection into the vitreous and in the needle track likely explain the intense fluorescence in the day 1 and 3 images. (**B**) Graph representing binding of fluorescently labeled MSCEVs to 50 µg of isolated vitreous humor coated to 96-well assay plates. The binding of MSCEVs to the vitreous humor was saturable. Data points represent mean ± SD (n = 6 experiments) of normalized fluorescence intensity..

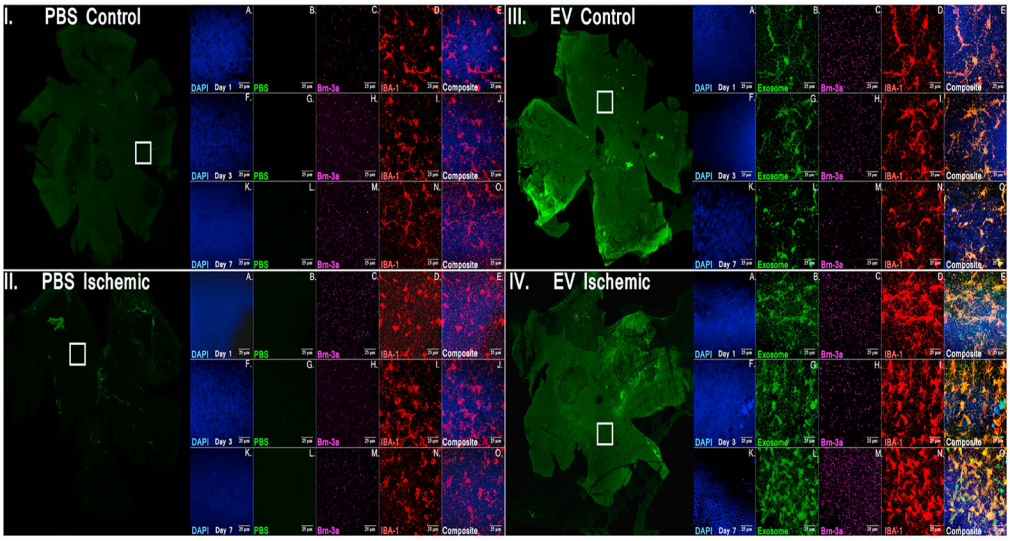

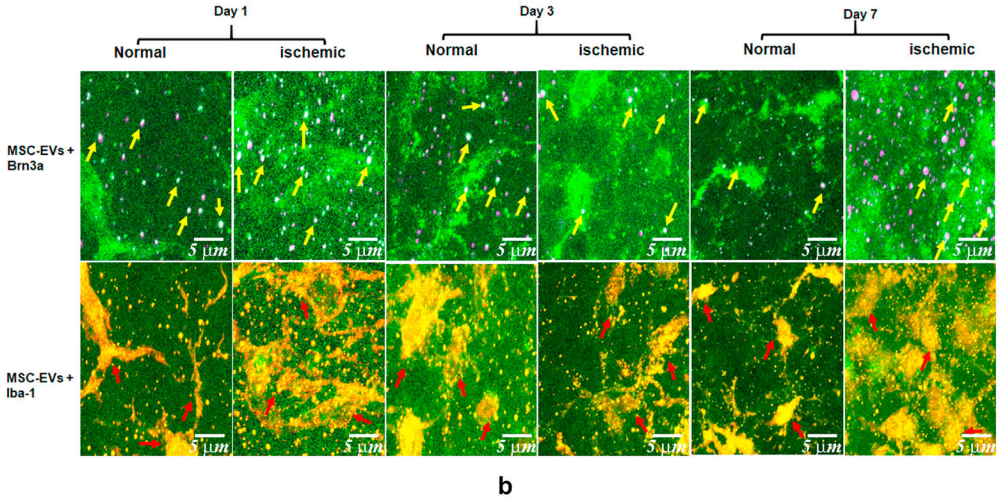

Fig 10. Uptake and distribution of MSC-EVs by normal and ischemic retinae *in vivo*:

(A) Flat mount confocal microscopic imaging of retinae injected with fluorescent MSC-EVs (green) and stained with retinal markers anti-Brn-3a for retinal ganglion cells (RGCs, magenta), anti-Iba-1 for microglia (red) and nuclei (DAPI, blue). Representative images displayed for days 1, 3 and 7 for PBS-injected control (**I**) and ischemic (**II**) retinae (left panel) and MSC-EV injected control (**III**) and ischemic (**IV**) retinae (right panel). For each group a low magnification image is presented in the green channel indicating the overview of the flat mount. The square white box indicates the representative area shown under higher magnification. Higher magnification images (63×) are provided in all channels followed by a merged image for days 1 (**A to E**), 3 (**F to J**) and 7 (**K to O**). Comparing (**III**) and (**IV**), enhanced MSC-EV uptake can be seen in the ischemic (**IV**) compared to the normal retina (**III**), along with enhanced co-localization with the activated microglia (red). The composite images (**E, J, and O**) for each group show co-localization of MSC-EVs and microglia

(yellow color, shown as white arrows in panel **IVE**), and Brn3a (white colored dots, shown by orange arrows in panel **IVE**), indicating that MSC-EVs were taken up by both RGCs and microglia after intravitreal administration. Blue arrows in panels **IID** and **IVD** show the greater amoeboid shape as opposed to ramified microglia indicating greater activation of microglia in ischemia-PBS injected compared to ischemia-MSC-EV injected retinae. N = 3 per time point. The uptake of MSC EVs by RGCs is further illustrated in (**B**), that are representative digital magnification of retinal flat mount images in (**A**) illustrating co-localization of MSC-EVs and distribution by specific retinal cell type in MSC-EV injected control and ischemic retinae, These images correspond to groups (**III**) and (**IV**) from (Fig 10A). Yellow arrows point to RGCs co-localized with MSC-EVs (green and magenta forming white, or white together with magenta, as Brn3a is a nuclear protein) and red arrows point to MSC-EVs with microglial cells (green and red forming yellow or orange).

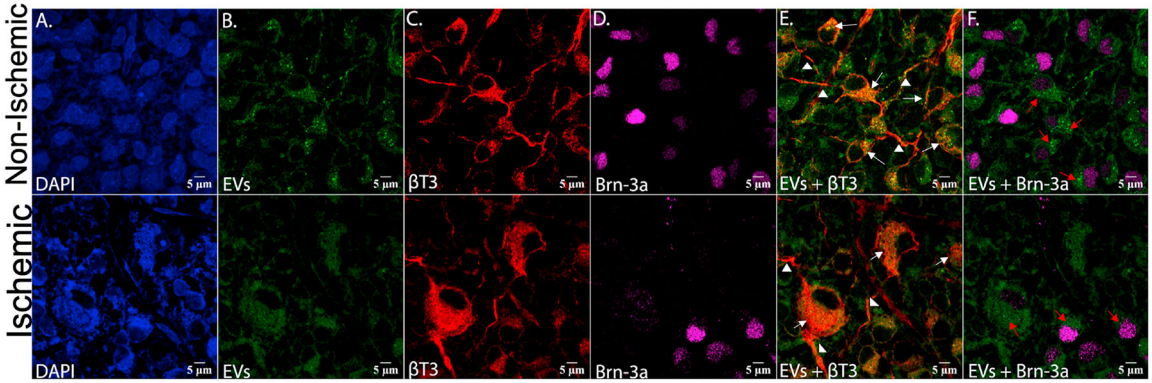

Fig 11. High magnification confocal imaging of retinal flat mounts shows that retinal neurons and retinal ganglion cells take up MSC-EVs, and that ischemia increases uptake.

Top panel shows control, non-ischemic retina, and bottom panel shows ischemic retina. Retinal flat mounts of non-ischemic eyes injected with green-labeled MSC-EVs, stained for **(A)** DAPI (blue), **(B)** EVs alone (green), **(C)** Beta-tubulin III alone (βT3, red), and **(D)** Brn-3a alone (magenta), **(E)** EVs (green) + βT3 (red), and **F)** EVs (green) + Brn-3a (magenta). βT3 stains only neurons and their axonal or dendritic projections. These flat mounts are from retinas harvested 24 h after injection of MSC-EVs, which was 48 h after ischemia. Red arrows in **F)** indicate the presence of EVs within the cell body of the retinal ganglion cells (Brn-3a stains only the nuclei of RGCs). Note that the majority of cells in **(B)**, **(E)**, and **(F)** show punctate green staining indicating that EVs were taken up by the cells. White arrows in **(E)** show the co-localization between the MSC-EVs and the retinal neuron cell bodies, indicated by the orange-yellow or orange color. White arrowheads mark the axonal or dendritic projections of the retinal neurons, and the presence therein of MSC-EVs **(E)**.

Table 1:

Antibodies Used

EM= electron microscopy
IF = immunofluorescence

	Manufacturer Name	Antibody Type	Primary Antibody Dilution
CD63, CD9, CD81, HSP70α	Abeam, Cambridge, MA, USA System Biosciences, Palo Alto, CA	Rabbit polyclonal, Mouse monoclonal	1:250 or 1:1000 Western blot (WB), electron microscopy (EM)
IL-6	Santa Cruz Biotechnology, Inc., Dallas, TX, USA	Mouse Monoclonal	1:500 WB
TNF-α	Santa Cruz Biotechnology	Mouse Monoclonal	1:500 WB
IL-1 β	Santa Cruz Biotechnology	Goat Polyclonal	1:500 WB
Caspase 3	Cell Signaling Technology, Danvers, MA, USA	Rabbit Polyclonal	1:1000 WB
β-actin	Sigma-Aldrich, St. Louis, MO, USA	Monoclonal mouse peroxidase conjugated	1:25000 WB
β-tubulin III	Sigma-Aldrich	Mouse monoclonal	1:5000 immunofluorescence (IF)
Caveolin-1	Santa Cruz Biotechnology	Rabbit polyclonal	1:1000 IF
Clathrin	Santa Cruz Biotechnology	Rabbit polyclonal	1:500 IF
IBA-1	Novus Biologicals, Littleton, CO, USA	Rabbit polyclonal	1:500 IF
Brn-3a	EMD Millipore (Millipore Sigma), Burlington, MA, USA	Rabbit polyclonal	1:500 IF